creative commons
COMMONS DEED

저작자표시-비영리-변경금지 2.0 대한민국

이용자는 아래의 조건을 따르는 경우에 한하여 자유롭게

- 이 저작물을 복제, 배포, 전송, 전시, 공연 및 방송할 수 있습니다.

다음과 같은 조건을 따라야 합니다:

저작자표시. 귀하는 원저작자를 표시하여야 합니다.

비영리. 귀하는 이 저작물을 영리 목적으로 이용할 수 없습니다.

변경금지. 귀하는 이 저작물을 개작, 변형 또는 가공할 수 없습니다.

- 귀하는, 이 저작물의 재이용이나 배포의 경우, 이 저작물에 적용된 이용허락조건을 명확하게 나타내어야 합니다.
- 저작권자로부터 별도의 허가를 받으면 이러한 조건들은 적용되지 않습니다.

저작권법에 따른 이용자의 권리는 위의 내용에 의하여 영향을 받지 않습니다.

이것은 이용허락규약(Legal Code)을 이해하기 쉽게 요약한 것입니다.

Disclaimer

dCollection

의학박사 학위논문

PI3Kγδ inhibitor plus radiation reinforces the antitumor immune effect of PD-1 blockade in syngenic and humanized triple-negative breast cancer model

삼중음성유방암 모델에서 PI3Kγδ저해제와
방사선 병용치료를 통한 PD-1억제제의
항종양면역효과 극대화 전략

2022년 8월

서울대학교 대학원

협동과정 종양생물학 전공

한 민 국

A Thesis of the Degree of Doctor of Philosophy

PI3Kγδ inhibitor plus radiation reinforces the antitumor immune effect of PD-1 blockade in syngenic and humanized triple-negative breast cancer model

삼중음성유방암 모델에서 PI3Kγδ저해제와
방사선 병용치료를 통한 PD-1억제제의
항종양면역효과 극대화 전략

August 2022

Interdisciplinary Program in Cancer Biology Major
The Graduate School
Seoul National University
Min Guk Han

PI3Kγδ inhibitor plus radiation reinforces the antitumor immune effect of PD-1 blockade in syngenic and humanized triple-negative breast cancer model

지도교수 김 인 아

이 논문을 의학박사 학위논문으로 제출함

2022년 4월

서울대학교 대학원

협동과정 종양생물학 전공

한 민 국

한민국의 박사학위논문을 인준함

2022년 7월

위 원 장 우 홍 균

부위원장 김 인 아

위 원 한 원 식

위 원 박 소 연

위 원 박 경 화

Abstract

Min Guk Han

Interdisciplinary Program in Cancer Biology Major
The Graduate School
Seoul National University

Introduction: The poor response of breast cancer to immune checkpoint blockade may result from low immunogenicity and the immune-suppressive tumor microenvironment. We hypothesized that combined use of phosphoinositide 3-kinase (PI3K) inhibitor to obstruct immune suppression and radiation therapy (RT) as a *in situ* tumor vaccination would reinforce the antitumor immune effect of PD-1 blockade as an immune checkpoint blockade.

Methods: Murine breast cancer cells (4T1) were grown in both immune-competent and immune-deficient BALB/c mice, and tumors were irradiated by 3 fractions of 24 Gy. A PD-1 blockade and a PI3Kγδ inhibitor were then administered every other day for 2 weeks. Flow cytometry analysis and immunohistochemistry served to monitor subsequent changes in immune cell population. Same experiments were performed in humanized patient-derived breast cancer xenograft (Hu-PDX) model, and its RNA of tumor was sequenced to identify immune-related pathways and to profile infiltrated immune cells.

Transcriptomic and clinical data were acquired from The Cancer Genome Atlas (TCGA) pan-cancer cohort, and the deconvolution algorithm was used to profile immune cell repertoire.

Results: The triple combination of RT, PD-1 blockade, and PI3Kγδ inhibitor significantly delayed tumor growth, boosted the abscopal effect, and improved animal survival. RT significantly increased $CD8^+$ cytotoxic T-cell fractions, immune-suppressive Tregs, MDSCs, and M2 tumor associated macrophages (TAMs). However, PI3Kγδ inhibitor significantly lowered proportions of Tregs, MDSCs, and M2 TAMs, achieving dramatic gains in splenic, nodal, and tumor $CD8^+$ T-cell populations after triple combination therapy. In a humanized PDX model, triple combination therapy significantly delayed tumor growth and decreased immune suppressive pathways. In TCGA cohort, high Treg/$CD8^+$ T cell and M2/M1 TAM ratios were associated with poor overall patient survival.

Conclusion: These findings indicate PI3Kγδ are clinically relevant targets in an immunosuppressive TME. And combining RT and PD-1 blockade may overcome the therapeutic resistance of immunologically cold tumors such as breast cancer having immunosuppressive tumor microenvironment.

Keywords : Breast cancer, PI3K inhibitor, Radiation therapy, PD-1 blockade, Immunotherapy, Abscopal effect
Student number : 2019-38319

Contents

List of Tables

List of Figures

I. Introduction

Immune checkpoint blockades (ICBs) improve outcomes of patients with solid tumors, such as malignant melanoma [1] and non-small cell lung cancer [2]. However, use of ICB monotherapy has limited efficacy for many other tumors [3]. Especially, the response rates in triple-negative breast cancer (TNBC) to ICB monotherapy are low, ranging from 5% to 21% [4,5]. One major potential mechanism of therapeutic resistance is the immune-suppressive tumor microenvironment (TME) characterized by dominance of immune-suppressive immune cells such as regulatory T cells (Tregs) [6], myeloid-derived suppressor cells (MDSCs), and M2 tumor-associated macrophages (TAMs) [7,8]. These immune cells impair the functions of anti-tumor immune cells, such as $CD8^+$ cytotoxic T cells, and thereby limit ICBs efficacy. Although TNBC is more immunogenic with higher levels of tumor-infiltrating lymphocytes, TNBCs with immune-suppressive TME indeed showed resistance to ICBs [9]. Study findings about infiltrating T cell-mediated tumor killing [10] indicate that depletion of immune-suppressive immune cells and promotion of anti-tumor T cell infiltration in the TME are key factors that enhance ICBs efficacy [11,12]. With respect to infiltrating T cells, breast cancer is generally regarded as an immunologically “cold” tumor characterized by relatively low infiltration of $CD8^+$ cytotoxic T cells and a low tumor mutational burden [13]. Thus, modulating TME susceptibility to

immunotherapy via combination with other treatment modalities is a promising strategy.

Radiation therapy (RT) can enhance the anti-tumor immune response by releasing tumor-associated antigens and priming T cells [3]. When coupled with ICBs [14,15], this *in situ* tumor vaccination effect is expected to result in control of unirradiated distant metastasis (i.e., the abscopal effect). RT can reprogram the TME by promoting effector T cell infiltration [16], which suggests that RT is a promising ICB partner [17]. With the recent success of ICBs in the treatment of advanced and metastatic cancers, whether it would be beneficial to combine RT and ICBs have become an important issue, with numerous clinical trials ongoing [18]. The synergistic effects of RT with ICBs are explained by the mechanism suggested for the immune-stimulatory effect of RT is immunogenic cell death, which involves the release of danger-associated molecular patterns (DAMPs) [19]. The DAMPs recruit and activate antigen-presenting cells and lead to the priming of the cytotoxic T cells [20]. Nevertheless, RT can also induce immunosuppressive responses by increasing Tregs, MDSCs, and M2 TAMs [21], which have central roles in adaptive immune resistance by deactivating tumor-specific cytotoxic T cells. Therefore, this is a reason why the immune-suppressive immune cells should be controlled by other inhibitors.

The phosphoinositide 3-kinase (PI3K) signaling molecule is an important immune regulator for cell survival, growth, and proliferation [22]. The PI3K family consists of three classes (I to III). Class I

PI3K molecules include a catalytic subunit (p110α, β, γ, or δ). Of these subunits, p110γ and p110δ are potential targets for tumor immune microenvironment modulation [23]. The PI3Kδ, which is the main isoform of PI3K activated by the T cell receptor [24], has been the target of clinical trials for treatment of hematologic malignancies [25]. A previous study using p110δ-inactivated mice found that inactivation of p110δ inhibits Treg and polymorphonuclear-MDSCs (PMN-MDSCs) function, which results in better tumor control and survival [23,26]. Solid-tumor 4T1 murine model findings indicate PI3K δ inhibitor impairs Treg function and releases $CD8^+$ cytotoxic T cells to result in a tumor suppression effect [23,26]. A selective PI3Kγ inhibitor can modulate the TME by shifting immunosuppressive M2-like to more inflammatory M1-like macrophages in a solid tumor mouse model [23,27]. Since adaptive immune resistance via Tregs, MDSCs, and M2 TAMs are the key components of resistance to ICBs, PI3K inhibitors could be a reasonable candidate as a target for combination therapy with programmed death protein 1 (PD-1) blockade [23]. Therefore, we hypothesized that targeting PI3Kγ, and PI3Kδ would be more effective to reverse immune suppressive TME.

Breast cancer is generally viewed as immunologically 'cold', imposing an immune-suppressive TME and responding poorly to lone ICB. As an adjunct to ICB, RT holds promise in terms of *in situ* tumor vaccination effect, although it is known to promote immune suppression, Tregs, MDSCs, and M2 TAMs. It was our contention that combined use of RT and a PI3Kγδ inhibitor to combat immune

suppression might enhance the efficacy of ICB (Figure 1). The objectives of this study were to examine the efficacy and mechanisms associated with using a combination approach of RT, PD-1 blockade, and selective inhibitor of PI3Kγδ (IPI-145, duvelisib) [23].

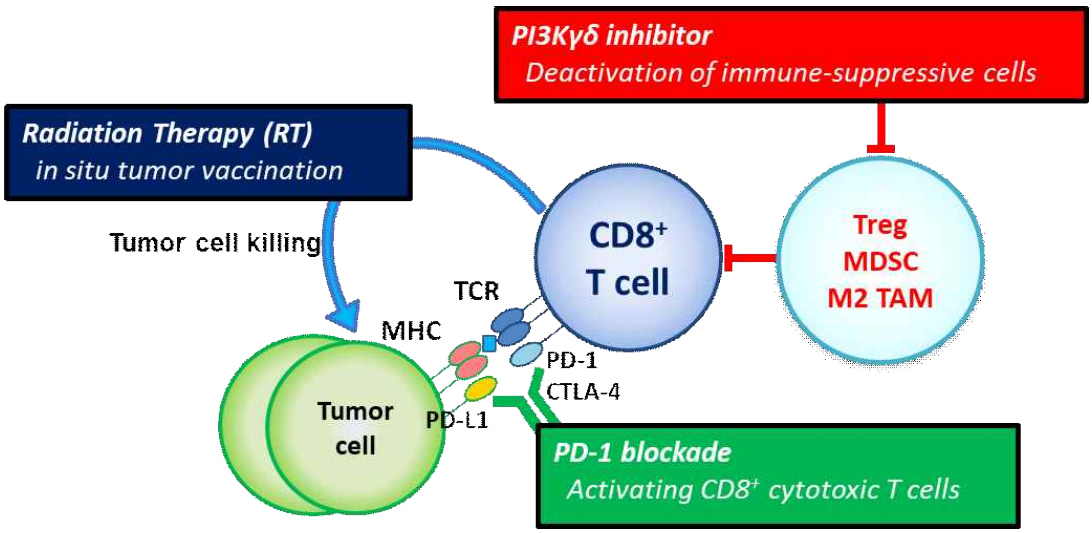

Figure 1. The strategic hypothesis.

This study aims to optimize the therapeutic effect of PD-1 blockade by deactivating immune suppressive cells using PI3Kγδ inhibitor, in addition to the *in situ* vaccination effect through RT. Abbreviations: MDSC = myeloid-derived suppressor cell; MHC= major histocompatibility complex; TAM = tumor associated macrophage; TCR = T-cell receptor; Treg = regulatory T cell.

II. Materials and Methods

1. Preparation of cell lines

Luciferase-tagged 4TI (4TI-luc) and untagged 4TI murine cancer cell lines for breast cancer were obtained from the American Type Culture Collection. The cells were maintained in culture plates using Dulbecco Modified Eagle Medium (DMEM, Corning) supplemented with 10% fetal bovine serum (Gibco, Invitrogen) and 1% penicillin (Welgene Inc) with streptomycin (complete DMEM medium). Cells were maintained at 37°C in 5% CO_2 humidified chambers.

2. *In vivo* studies using syngenic murine tumor model

Female Balb/c mice (6 weeks old) were purchased from Orient Bio Inc. (Sungnam, Korea). Mice were injected with 6×10^5 triple-negative breast cancer (TNBC) 4T1-luc or luciferase-untagged 4TI murine cells in the subcutaneous tissue of the right hind limb or left flank of the mice. Eight-week-old mice were used for all experiments. All mice were maintained and treated in accordance with the Institutional Animal Care and Use Committee regulations at the Clinical Research Institute, Seoul National University Bundang Hospital (IACUC approval number: BA1807-251/054-06, BA-2011-308-104-05). Each mouse was randomly assigned to one of eight groups: control, RT, PI3Kγδ inhibitor, PI3Kγδ inhibitor + RT, PD-1 blockade, PD-1 blockade + RT, PI3Kγδ inhibitor + PD-1 blockade, or triple combination. There were at least five mice per group in each experiment. Tumors were irradiated using a total dose

of 24 Gy given in 8 Gy three fractions. RT was delivered via an electron beam every 2 days for a week. Treatments were given as single agents or in combination using the following regimen. The PD-1 blockade was purchased from Biolegend (clone RMP1-14, 114115) and treated at 10 mg/kg. The PI3Kγδ inhibitor (Duvelisib, Selleckchem, S7028) given at 15 mg/kg. These drugs were injected via the intraperitoneal route once every 2 days for 2 weeks (Figure 2). Tumor size was measured periodically using a caliper, and total tumor volume (length × width^2 × 0.5) was calculated. Animals were euthanized when signs of distress were observed or when total tumor volume reached 1,000 mm^3 or up to 3,000 mm^3. Tumor progression was observed using an *in vivo* imaging system (IVIS). At the end of the study, the tumor, the spleen, and the inguinal lymph node as draining lymph node (dLN) were isolated from each mouse, and a portion of each tissue type was immediately fixed using 4% paraformaldehyde for immunohistochemistry study. The remaining tissues were minced with scissors before incubation with 100 U/ml collagenases (Gibco) and 0.2 mg/ml DNase (Roche) in Hank's Balanced Salt Solution (HBSS) for 30 min at 37 °C. The samples were homogenized using repeated pipetting and were filtered through a 70 μm cell strainer (Falcon) in supplemented RPMI to generate single-cell suspensions. After red blood cell lysis was accomplished using ACK Lysing Buffer (Gibco), all samples were washed and re-suspended in Cell Staining Buffer (Biolegend, 420201). Immune modulatory function was estimated using flow cytometry analysis (fluorescence activated cell sorting, FACS; FACSCalibur, BD Biosciences).

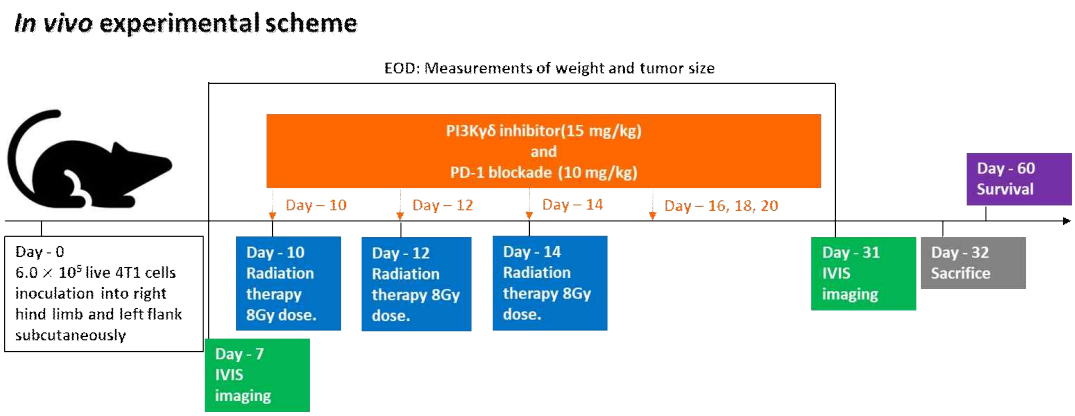

Figure 2. Treatment schedule for mice treated with RT, PD-1 blockade, and PI3Kγδ inhibitor.

This is the overall schedule for administering RT, PI3Kγδ inhibitor, and PD-1 blockade. The RT was performed using a total dose of 24 Gy given in 8 Gy in three fractions every other day. The PI3Kγδ inhibitor and PD-1 blockade were administered via the intraperitoneal route every 2 days for 2 weeks. Abbreviations: EOD = every other day.

3. Bioluminescence imaging

Bioluminescence images were obtained using the IVIS Imaging System 100 series (Xenogen Corporation) according to the manufacturer's protocol. Mice were injected with luciferin (Promega, 2.5 mg/mouse) 10 min before imaging under anesthesia (1 - 2% isoflurane). The acquired images included peak luminescence signals and were recorded for 10 min. Calculated values for relative tumor burden were analyzed using the statistical method presented in the Statistical Analysis section.

4. Immunohistochemistry and immunofluorescent staining, confocal microscopy

The tumor tissues isolated from mice were fixed with formalin and paraffin-embedded tissue blocks were constructed. The paraffin-embedded tissues were prepared and cut into serial 4-μm transverse sections. The sections were deparaffinized using a xylene-to-ethanol gradient and incubated with 3% H_2O_2 in methanol for 10 min at room temperature. Then, they were boiled in 0.01 M sodium citrate buffer (pH 6.0) for antigen retrieval and blocked with 5% normal goat serum (Vector Laboratories, Burlingame, CA). The processed sections were incubated at 4°C overnight with primary antibodies against the following: Santa Cruz Biotechnology: cGAS (sc515777), CD8 (sc-18860 AF488), FasL (sc-19681 AF647), PI3Kp110 γ (sc-166365) and PI3Kp110δ (sc-55589); Cell Signaling Technology: p-AKT (4060S) and FOXP3 (NoVus, NB100-39002); or Abcam: HIF-1α (ab16066), PD-L1 (ab2025921), CD8 (ab203035), CD31 (ab222783), CD163 (ab1822422), and Ly6G (ab25377). The ImmPRESS Goat Anti-Rat IgG (Mouse Adsorbed) Polymer kit (Vector

Laboratories), Abcam (ab150165, ab150081), and REAL EnVision detection system (Dako) were used for the secondary antibody and color development detection, respectively. Immunostained sections were counterstained with hematoxylin and mounted using Organo/Limonene mounting medium (Immunobioscience). These stained sections were observed at 40× magnification using an Axioskop 40 light microscope (Carl Zeiss) and AxioVision 4.7 software. Optical density was quantified using Image J software (NIH, Bethesda). The mean density of three slices per sample was calculated.

5. Flow cytometery analysis

Twenty days after tumor cell inoculation, the mice were euthanized and the draining lymph nodes, spleens, and tumors were isolated. Tumors were excised, and single-cell suspensions were obtained using mechanical processing and enzymatical digestion. Whole spleen and draining lymph node tissues were mechanically processed and stained upon erythrocyte lysis (Gibco™). Cells isolated from mouse tumors, spleens and dLN were pre-incubated (15 min, 4 °C). After each organ single-cell isolation procedure, the 1×10^6 cells per FACS tube were stained with Fc blocker (clone 2.4G, BD Biosciences) for block nonspecific binding and stained with appropriate dilutions of various combinations of the following fluorochrome-conjugated antibodies for 30 min, at 4 °C to analyze leukocyte infiltrates: BD Pharmingen: CD3 (555274), CD8b (550798), CD11b (553312), CD45 (553080), F4/80 (565410), and MHCII (562363) or Biolegend: CD4 (100405, 100511, 100539, 100515), Ly6G (127605), CD25 (102029), Ly6C (128011), CD8a (100733), CD127 (135021), and CD206 (141707). For

intracellular staining, cell surface marker staining was performed for 30 min on ice and intracellular FOXP3 (eBioscience, 12-5773-80) staining was performed according to the manufacturer's instructions (complete kit; eBioscience). Three or four colors were used simultaneously, which are FITC, PE, PerCP-Cy5.5, and APC. CD4 antibody was used for compensation for Treg and CD8 analysis, and CD11b antibody was used for MDSC and TAM analysis. For each analysis, different tubes were used and at least 3 replicates were performed. The data were acquired using FACSCalibur machines and analyzed using FlowJo software (Treestar, version 10).

6. Measurement of interferon (IFN) beta and gamma level

Blood samples were obtained from the intra-orbital vein using a micro hematocrit capillary tube, then centrifuged at 1,000 x g for 30 min at 25°C. The serum samples were immediately stored at −80 °C. According to manufacturer's protocol, 20 μl of 1:5 diluted serums were analyzed using Mouse ProcartaPlex™ Simplex Kit (Invitrogen™, EPX01B-26044-901 or EPX01A-20606-901) by Luminex to measure serum IFN-β and IFN-ɣ levels. The quantification of concentraion of IFN-β and IFN-ɣ performed by using the Bio-Plex® 200 Systems and the Luminex xPONENT Software (Luminex Corporation) on the basis of corresponding standards curves.

7. Generation of humanized patient-derived xenograft (PDX) model

Humanized mouse models (HuNSG; human $CD34^+$ hematopoietic stem cell-engrafted NOD.Cg-Prkdcscid Il2rgtm1Wjl/SzJ mice [NSG™]), which included multi-lineage human immune cells, were purchased from The Jackson Laboratory (Bar Harbor, Maine, USA). HuNSG mice that had > 50% $hCD45^+$ cells in the peripheral blood were measured in The Jackson Laboratory report as humanized mice. Patient breast cancer tissues (IRB approval number: C-1402-054-555) were obtained from surgical specimens of patients with breast cancer tumors showing high expression of PI3Kγ and δ at Ewha Woman's University Hospital. Humanized PDX models were generated via implantation into the HuNSG mice (IACUC approval number: BA1906-274/036-01, IBC approval number: IBC-2005-R-009-01). Since the human immune system in humanized NSG mice has been reported to be maintained for 6 weeks [28], we transplanted the patient-derived tumors and conducted whole experiments within 7 weeks. Patient-derived tumors were minced into 1×1.5×1.5 mm^3 pieces and loaded into humanized mouse models. The minced tumor tissue was transplanted subcutaneously into the right flanks of HuNSG mice while under isoflurane gas anesthesia. Tumor size was measured three times a week after tumor transplantation. The experiment was completed when the tumor volume reached 1,000 mm^3. All mice were maintained according to guidelines established by the Institutional Animal Care and Use Committee.

8. Humanized PDX-derived tumor mRNA sequencing and bioinformatic analysis.

Tumor was collected from one humanized PDX mice in each eight group: control, RT, PI3Kγδ inhibitor, PI3Kγδ inhibitor + RT, PD-1 blockade, PD-1 blockade + RT, PI3Kγδ inhibitor + PD-1 blockade and triple combination. Tumor RNA was extracted from whole embryos using RNeasy Mini Kit (QIAGEN, 74104). mRNA quality was assessed using the RNA 6000 Nano-Assay on a BioAnalyser 2100 (Agilent Technologies). We performed TruSeq RNA Sample Prep Kit v2 (Illumina) and paired-end sequencing (Illumina HiSeq 4000; 101-bp reads; 6.3 - 7.4 Gb), trimming (Trim Galore) and alignment of reads to the human genome hg19 (Hisat2 and STAR aligner), gene quantification (StringTie), gene counts (HTseq-count). To reduce sample-to-sample systematic bias that may affect the interpretation, the data were calibrated by Trimmed Mean of M-values (TMM) normalization and estimating the size factor using count data in 'edgeR' R package library. Gene ontology (GO) enrichment analysis was performed by using 'g:Profiler' (https://biit.cs.ut.ee/gprofiler/). Compared with control group, -log10 false discovery rate (FDR) was calculated in terms of immune-related GO terms. Gene set variation analysis was performed by using 'gsva' R package with gene signatures related with immune response or treatment response. Compared with the control group, P-values were calculated in terms of KEGG canonical pathways. Gene set variation analysis (GSVA) was performed using the gsva R package with canonical gene signatures that were retrieved from the Reactome [29] , Biocarta [30], and KEGG databases. The CIBERSORTx deconvolution method [31] was used to estimate infiltrated immune cells within the TME.

9. TCGA data acquisition, immune cell deconvolution, and survival analysis

Transcriptomic and clinical data were acquired from the TCGA pan-cancer cohort through the Xena browser (https://xenabrowser.net/datapages) platform. A batch-normalized mRNA sequencing count dataset (N=11,069) was used for immune cell deconvolution. To define PD-L1 high and low expression groups, we used the median CD274 mRNA expression value as a threshold. Patients with upper median value expression were grouped into the PD-L1 high group; those with lower median values were assigned to the PD-L1 low group. In a whole cohort, the Phosphatidylinositol-4,5-Bisphosphate 3-Kinase Catalytic Subunit Gamma (*PIK3CG*) or Phosphatidylinositol-4,5-Bisphosphate 3-Kinase Catalytic Subunit Delta (*PIK3CD*) high expression groups were defined as the upper median of each mRNA expression value; the low expression groups were defined as the lower median value for each. Using by the xCell [32], we analyzed fractions of four immune cells, including CD8+ T cells, M1 TAMs, M2 TAMs, and Treg. fractions of these immune cells plotted in bar graphs and represented in heatmaps. Tumor purity-adjusted ratios were calculated by inverse-weighting the immune score to the unadjusted ratio. To analyze survival, we selected samples with available OS data, removed duplicate samples within a patient, and matched with samples and survival data using the R program 3.6.1 version. High-quality survival data was obtained from a previous study [33]. For the survival analysis, we analyzed data from 10,844 TCGA pan-cancer cohort patients.

10. Statistical Analysis

The statistical analysis were performed using GraphPad PRISM statistical analysis and graphing software (GraphPad 8). To analyze tumor growth curves as a function of time, we fitted a linear mixed effect model with a restricted maximum likelihood function. After computing differences in predictive margins among groups, we performed pairwise comparisons. For the pairwise comparisons, P-values were calculated with adjustment of the comparison-wise error rate based on the upper limit of the Bonferroni inequality. In terms of tumor volume or burden, t-tests were performed, and the results were presented as mean ± standard error of the mean (SEM) values calculated from the results for at least three animals in each group, unless otherwise noted. A P-value < 0.05 was considered statistically significant (*, $P < 0.05$; **, $P < 0.01$; ***, $P < 0.001$; ****, $P < 0.0001$). Each immune cell fraction was plotted in a scatter bar plot according to subgroup. One sample t-tests were performed to test whether a mean immune cell fraction was not statistically zero. Wilcoxon rank-sum tests were performed to compare median fractions of immune cells between groups. Kaplan-Meier curves were plotted and log-rank tests were performed using STATA 15.

II. Results

1. Combining RT and PI3Kγδ inhibitor with PD-1 blockade resulted in enhanced antitumor effects

We inoculated 4T1-luc murine TNBC cell-lines into subcutaneous tissue in syngenic mice, then we measured tumor volume in each group to assess the antitumor effect. Figure 3 presents the results for tumor volume growth delay curves for each group. Of the treatment groups, using triple combination therapy, PD-1 blockade + RT + PI3K γδ inhibitor, resulted in the greatest anti-tumor effects ($P < 0.001$), compared with the control group. A pairwise comparison analysis revealed there were no significant mean tumor growth differences between the RT and PI3Kγδ inhibitor + PD-1 blockade groups ($P=0.077$) or between the PD-1 blockade and PI3Kγδ inhibitor + PD-1 blockade groups ($P=0.244$). We used bioluminescence imaging to measure tumor burdens before (10 days after inoculation) and after intervention (31 days after inoculation) (Figure 4). Consistent with the tumor volume results, use of the triple combination therapy resulted in the most tumor burden suppression. Observation of mice for an extended period of up to 45 days revealed that the tumor growth rate in the PD-1 blockade group accelerated 7 days after treatment had been stopped (Figure 5). The triple combination group had the longest mean survival, up to 50 days, followed by the PD-1 blockade + RT and PI3Kγδ inhibitor + RT combination groups (Figure 6). Mice treated using the triple combination had the smallest tumor sizes, even up to 42 days after inoculation (Figure 7). The mice in the group with hyperprogression following PD-1 blockade had the

worst survival (Figure 5). This hyperprogression was also visually apparent in terms of tumor burden (Figure 7).

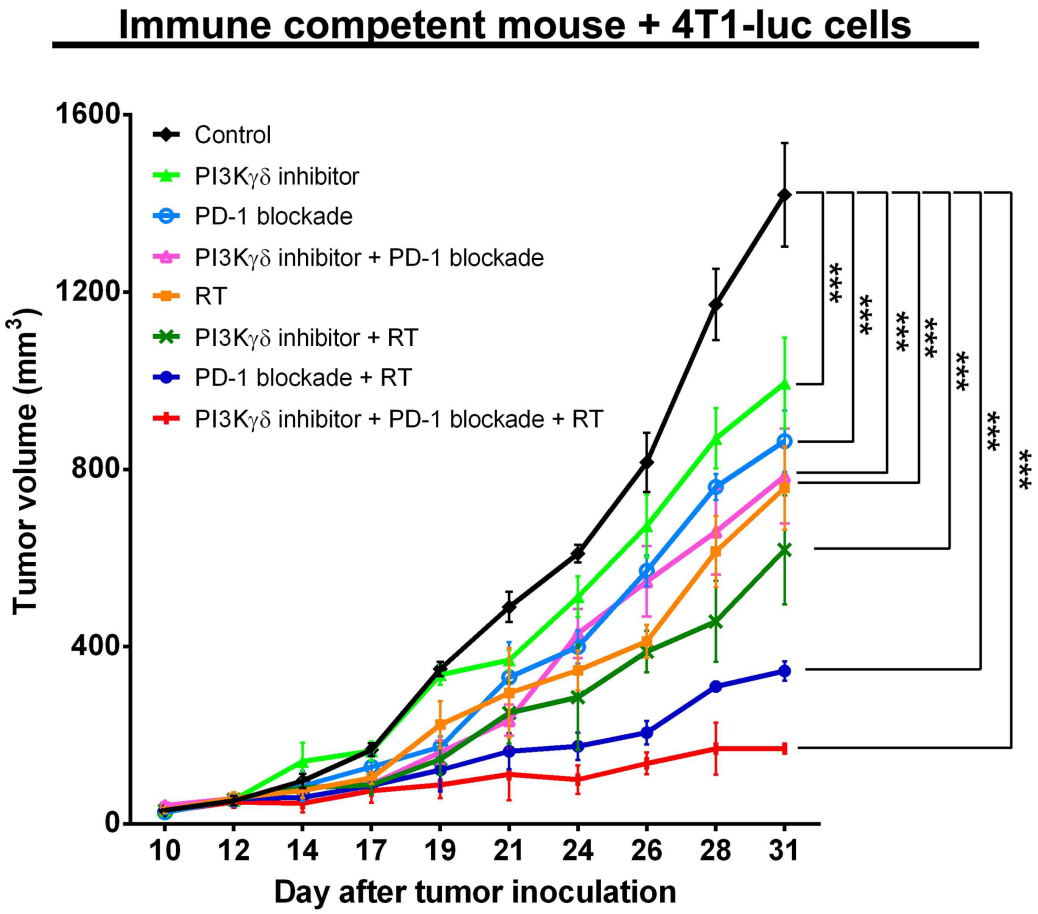

Figure 3. Tumor growth curves of subcutaneous implants in mice in each groups.

The graph presents the results of growth tumor volume which was measured for 31 days for each group. Each group measured statistical values compared with the control group. ***, $P < 0.001$. Abbreviations: RT = radiation therapy.

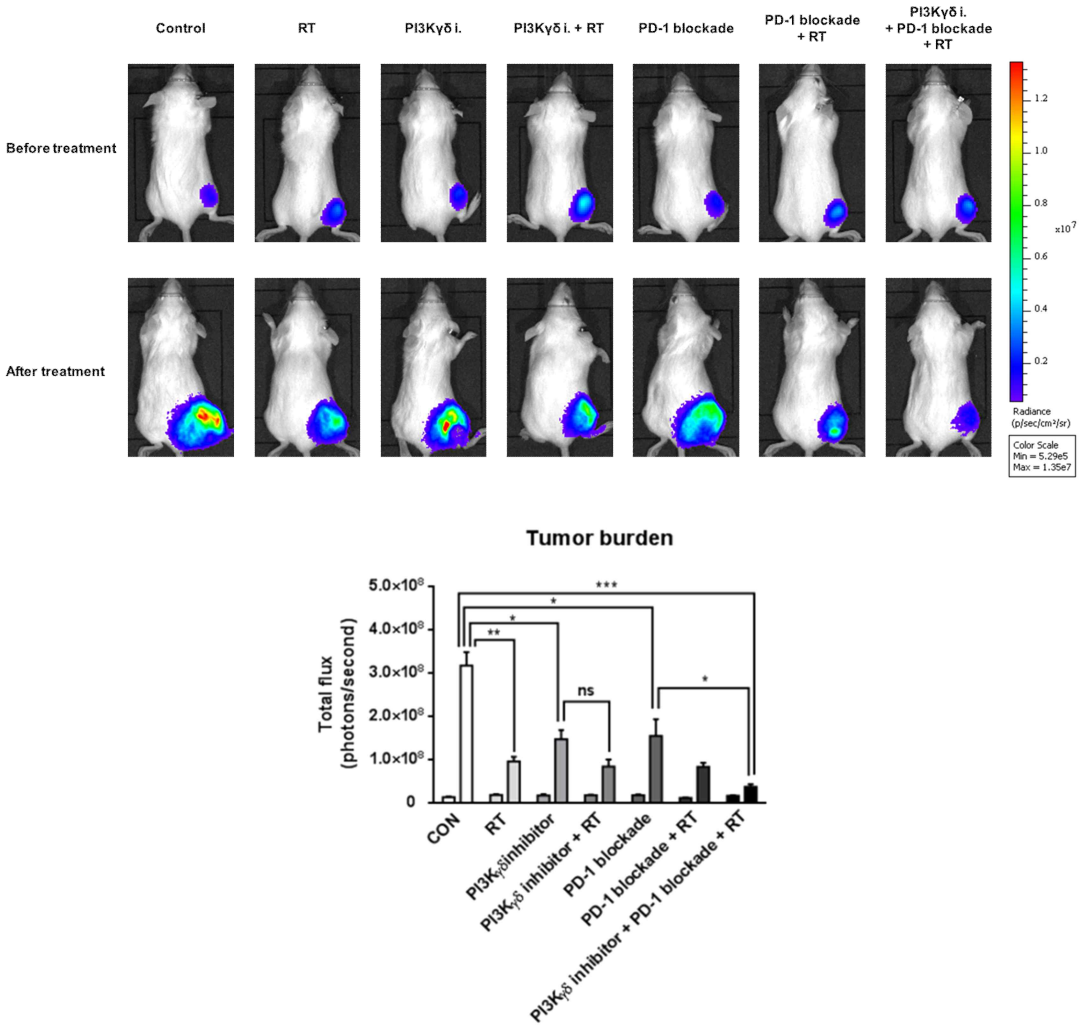

Figure 4. Representative bioluminescence images and graph

The Representative bioluminescence images were obtained before (Day 7) and after (Day 31) each treatment after subcutaneous inoculation of 4T1-luc tumor cells for each group. The luminous intensity of photons emitted from each tumor in the images was quantified in graph. *, $P < 0.05$; **, $P < 0.01$; ***, $P < 0.001$; ns, not significant. Abbreviations: CON = control; i. = inhibitor; RT = radiation therapy.

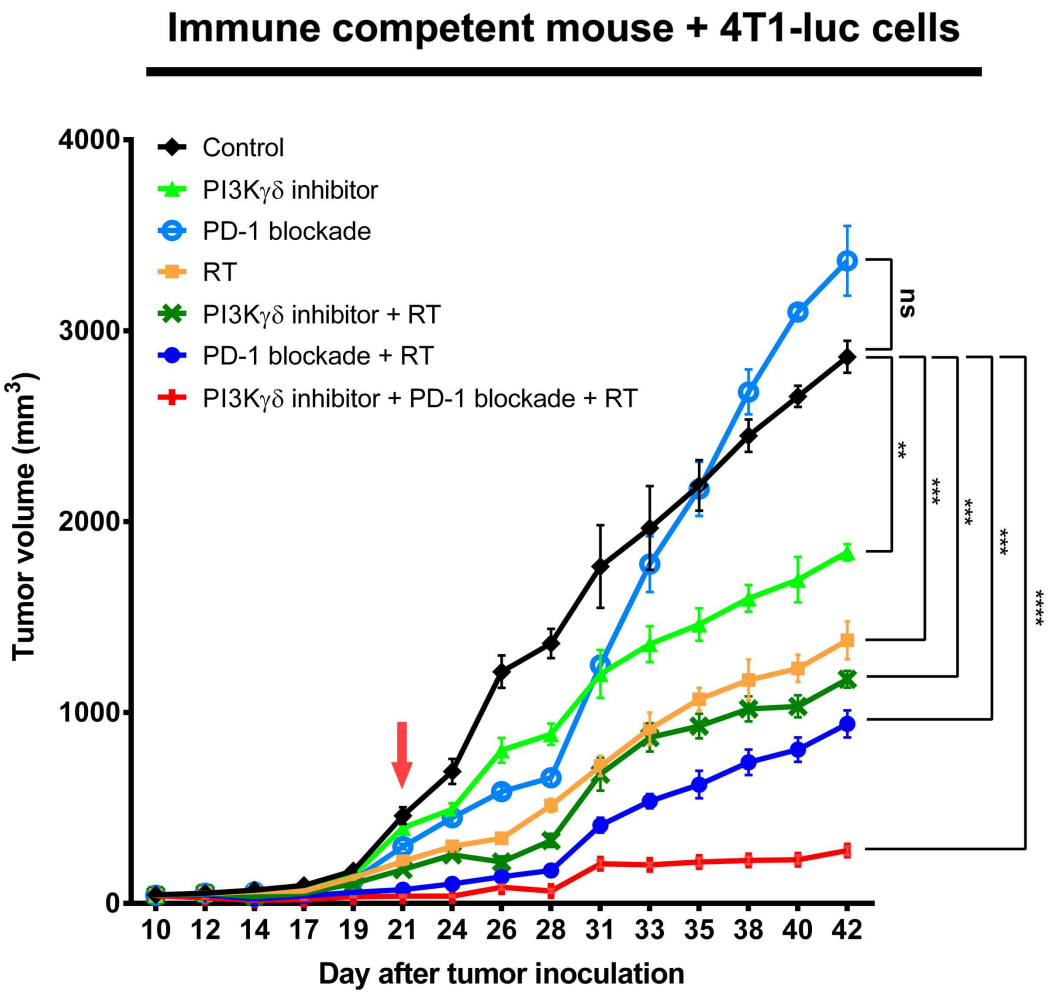

Figure 5. Tumor growth curves of subcutaneous implants in mice in each groups for an extended period of up to 45 days.

The graph presents the results for growth tumor volume which was measured for even up to 42 days after inoculation for each group. Each group measured statistical values compared with the control group. Red arrows indicate the termination of drug treatment. **, $P < 0.01$; ***, $P < 0.001$; ****, $P < 0.0001$; ns, not significant. Abbreviations: RT = radiation therapy.

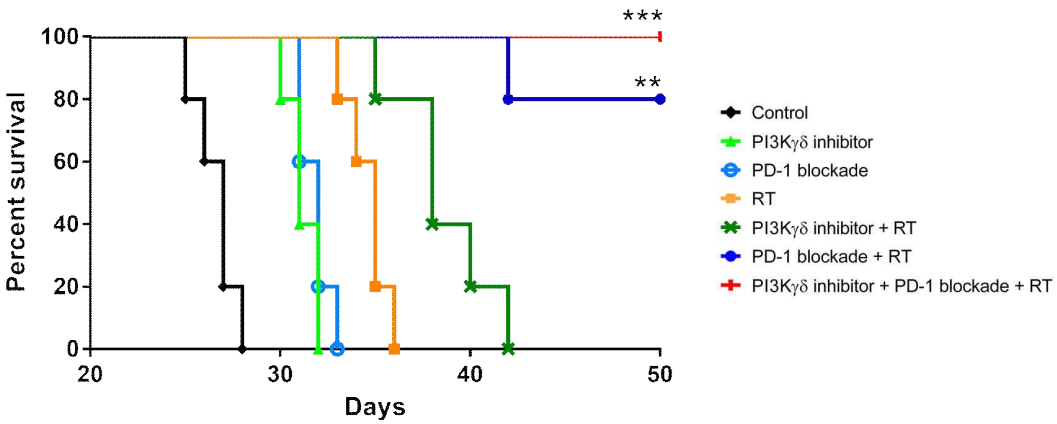

Figure 6. Survival of 4T1 tumor-bearing mice in each groups.

The graph presents the results for the survival rate recorded for 50 days (n=5). The 4T1 tumor-bearing mice treated with RT, PI3Kγδ inhibitor, PI3K γδ inhibitor combined RT, PD-1 blockade, PD-1 blockade + RT, PI3Kγδ inhibitor + RT, or triple combination, compared with the control group. **, $P < 0.01$; ***, $P < 0.001$. Abbreviations: RT = radiation therapy.

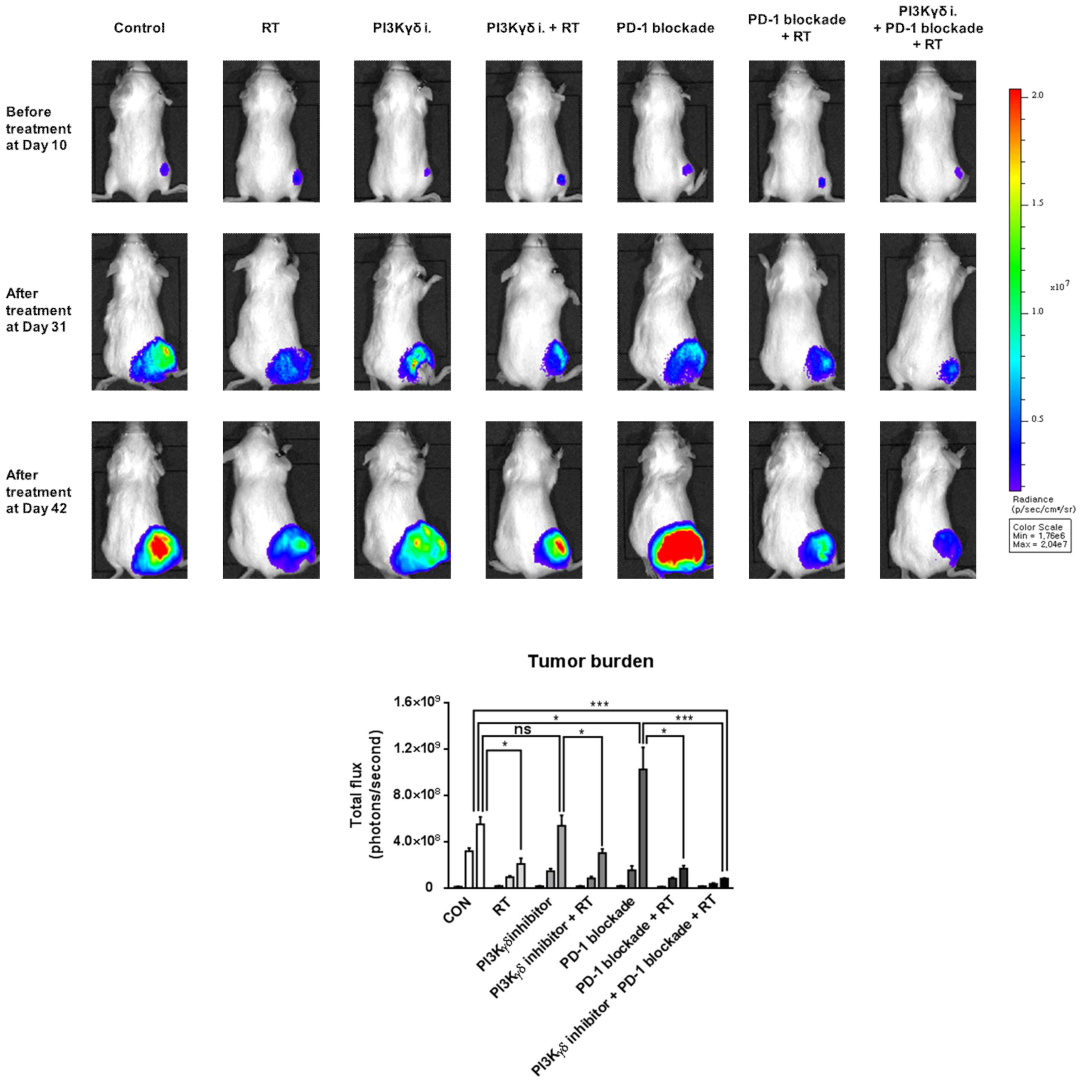

Figure 7. Representative bioluminescence images and graph for an extended period of up to 42 days.

The Representative bioluminescence images were obtained before and after each treatment even up to 42 days after inoculation for each group. The luminous intensity of photons emitted from each tumor in the images was quantified in graph. *, $P < 0.05$; ***, $P < 0.001$; ns, not significant. Abbreviations: CON = control; i. = inhibitor; RT = radiation therapy.

2. Abscopal effects

Given that the abscopal effect following local RT administration is driven by the immunogenic response, we hypothesized that an enhanced anti-tumor immune response from triple combination therapy could suppress growth of unirradiated distant tumors. To evaluate the abscopal effect, 4T1-luc tumor cells were inoculated in the right hind limb as the primary tumor and in the left flank as the secondary tumor. After the primary tumor was irradiated, growth of the unirradiated secondary tumor was measured using bioluminescence imaging (Figure 8). The results indicated that use of triple combination therapy significantly delayed unirradiated secondary tumor ($P<0.01$) and primary tumor ($P<0.01$) growth (Figure 8).

The immune response can be elicited using luciferase-specific $CD8^+$ T cells [34,35]. To exclude a luciferase-driven confounding effect during the abscopal response, we performed the same experiment using luciferase-untagged 4T1 cells and found a similar pattern of tumor growth delay (Figure 9). We found the most superior primary and secondary tumor control in the triple combination group, even for luciferase-untagged 4T1 cells. The results for unirradiated secondary tumors indicated there were no significant differences in mean tumor volumes between the PD-1 blockade vs. control ($P=1.000$), PD-1 blockade vs. PI3Kγδ inhibitor ($P=0.188$), PI3Kγδ inhibitor vs. PI3Kγδ inhibitor + PD-1 blockade ($P=1.000$), PI3Kγδ inhibitor + PD-1 blockade vs. RT ($P=0.206$), and PI3Kγδ inhibitor + RT vs. PD-1 blockade + RT ($P=1.000$) groups.

To verify that an intact immune response was required for an effective abscopal effect, we tested whether both primary and secondary tumors were controlled in immune-compromised nude mice (Figure 10). Although use of the triple combination treatment resulted

in the most superior anti-tumor effect, there were no significant tumor volume differences among the RT, PI3Kγδ inhibitor + RT, and triple combination groups (all pairwise-adjusted P=1.000). The results for the unirradiated secondary tumors (Figure 10), volumes, and growth curve patterns were almost the same among all groups. Thus, the enhanced anti-tumor effects using triple combination therapy to delay primary and secondary tumor growth were not found in immune-deficient mice.

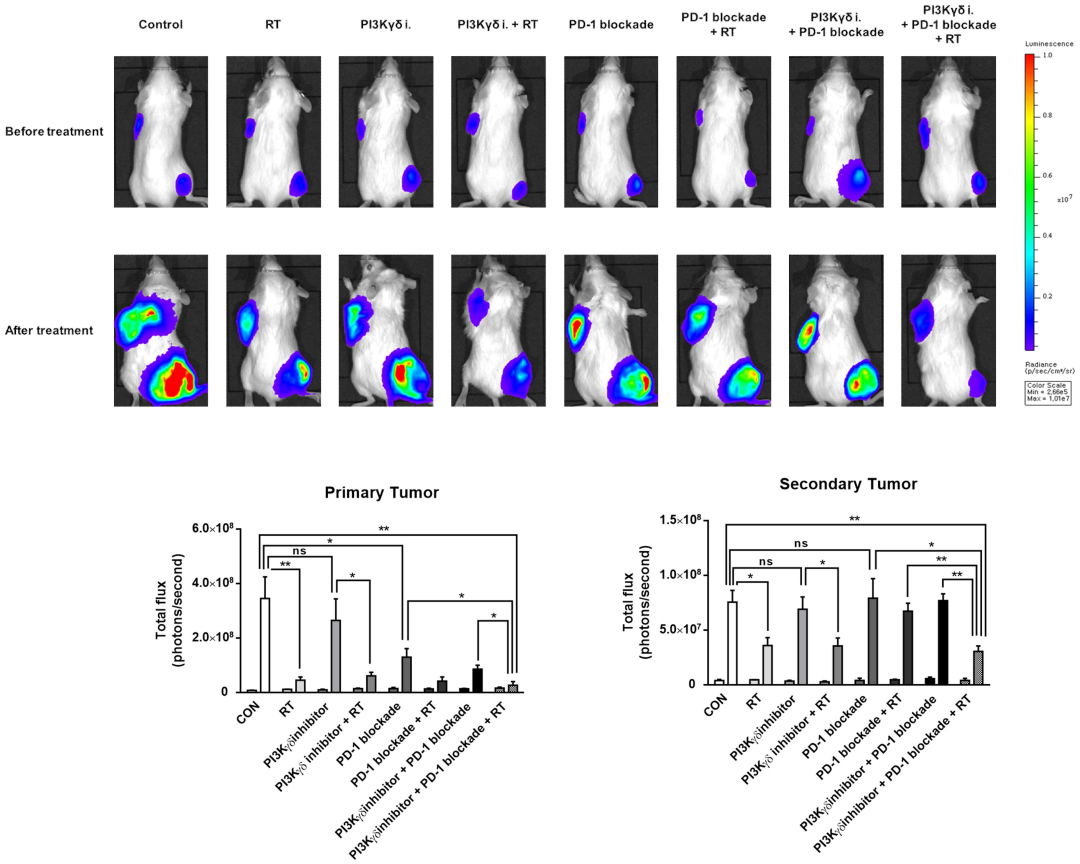

Figure 8. Representative bioluminescence images were obtained before and after each treatment, after subcutaneous inoculation of 4T1-luc tumor cells.

Relative tumor burdens of tumor inoculated into the primary tumor (right hind limb) and secondary tumor (left flank) sites. The luminous intensity of photons emitted from each tumor in the images was quantified in graph. *, $P < 0.05$; **, $P < 0.01$; ns, not significant. Abbreviations: CON = control; i. = inhibitor; RT = radiation therapy.

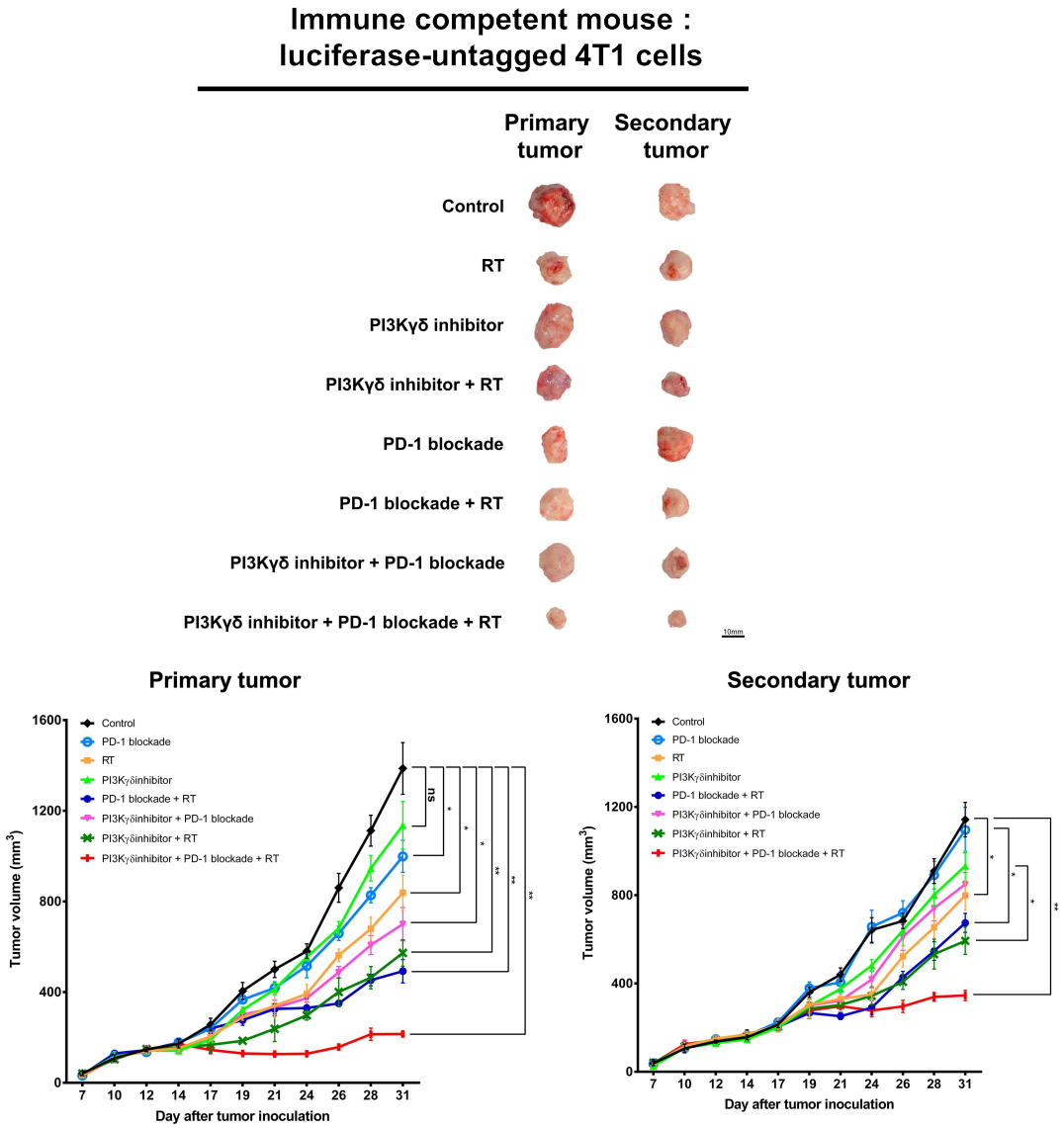

Figure 9. Gross tumors and tumor growth curves in luciferase-untagged 4T1 tumor-bearing mice.

The representative tumor images at the end of the experiment (day 31) and tumor growth curves for the right hind limb (the primary tumor) and left flank (secondary tumor) sites were presented in luciferase-untagged 4T1 tumor-bearing mice. *, $P < 0.05$; **, $P < 0.01$; ns, not significant. Abbreviations: RT = radiation therapy.

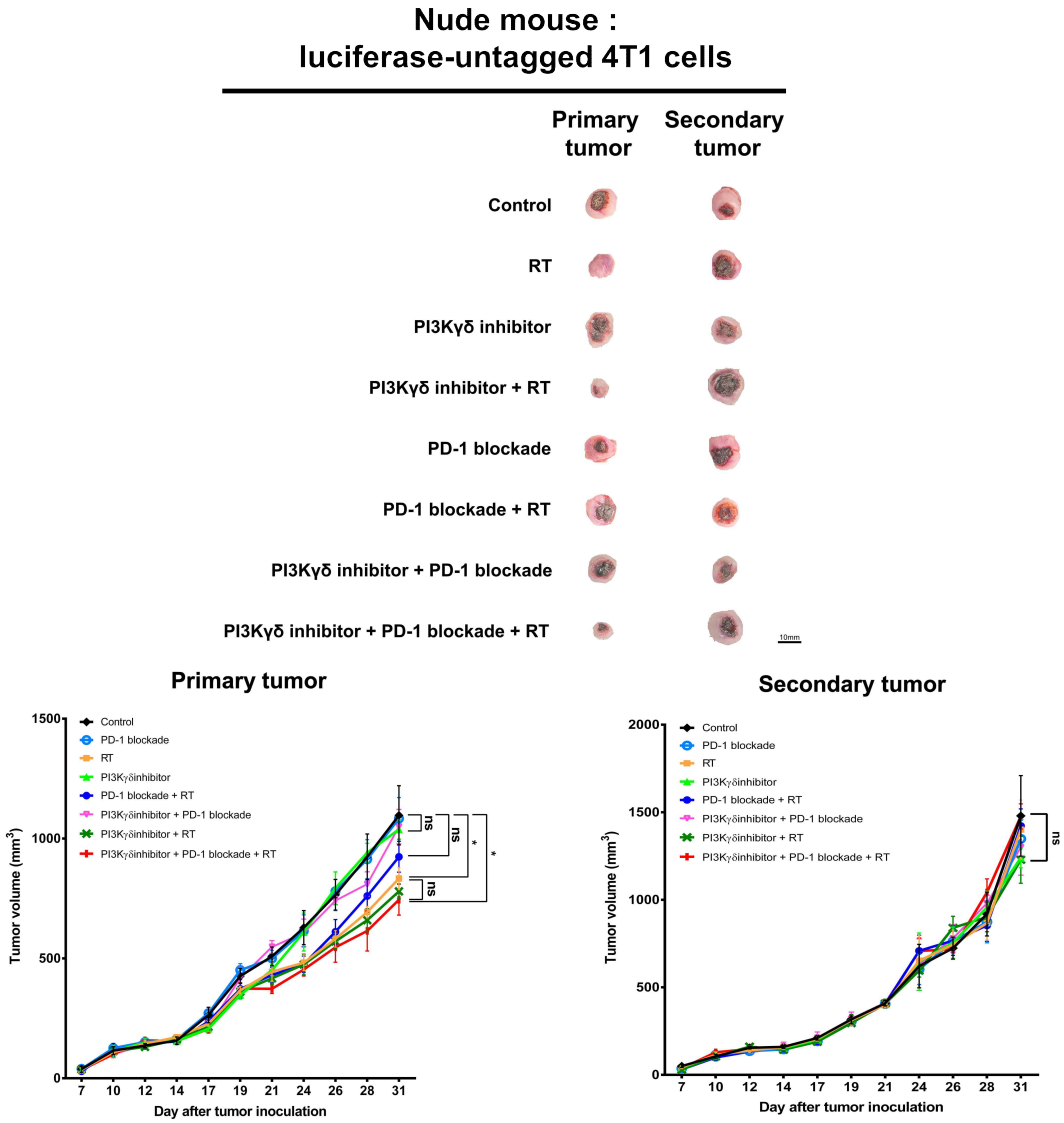

Figure 10. Gross tumors and tumor growth curves in nude mice.

The representative tumor images at the end of the experiment (day 31) and tumor growth curves for the right hind limb (the primary tumor) and left flank (secondary tumor) sites were presented in luciferase-untagged 4T1 tumor-bearing nude mice. *, $P < 0.05$; ns, not significant. Abbreviations: RT = radiation therapy.

3. Expression of key molecules according to treatment

Levels of phosphorylated protein kinase B (p-AKT), programmed death-ligand 1 (PD-L1), and cyclic GMP-AMP synthase (cGAS) were examined using immunohistochemistry. We first found decreased PI3K γ and PI3Kδ protein levels by PI3Kγδ inhibitor in tumor cells (Figure 11A, B). Then, we examined levels of p-AKT, which is the surrogate marker for downstream inhibition in the PI3K/AKT/mammalian target of rapamycin (mTOR) signaling pathway [36]. PI3Kγδ inhibitor significantly downregulated pAKT, which is a key downstream effector of PI3K (Figure 12A). Next, we tested PD-L1 expression according to treatment group (Figure 12B). RT increased PD-L1 expression, and PI3Kγδ inhibitor or PD-1 blockade downregulated PD-L1 expression. Of all treatment groups, the triple combination group had the lowest mean level of PD-L1 expression. We also examined hypoxia-inducible factor 1-alpha (HIF-1α) protein expression (Figure 12C); it was not affected by use of RT alone but was decreased by use of PI3Kγδ inhibitor or PD-1 blockade.

We also examined whether 8 Gy × 3 fractions effectively induced cGAS expression, which is a downstream stimulator of the interferon (IFN) gene (STING) pathway. Irradiation with 8 Gy × 3 fractions significantly increased mean cGAS expression; the mean level was highest in the triple combination group (Figure 13). ELISA assays revealed increased serum levels of IFN-β (Figure 14, left panel) and IFN-γ (Figure 28, right panel). This finding suggested this dose-fractionation resulted in effective immune stimulation.

Fas-ligand (FasL) expression on tumor endothelial cells [37] and polymorphonuclear myeloid derived suppressor cells (PMN-MDSCs) [38] can suppress tumor infiltrating T cells. Thus, we performed

immunofluorescent staining of endothelium (CD31, Figure 15A), PMN-MDSCs (Ly6G, Figure 15B), M2 TAMs (CD163, Figure 15C), and CD8+ T cells (CD8, Figure 15D) with co-staining of FasL. In the triple combination group, we found decreased FasL expression in the tumor endothelium, PMN-MDSCs, and M2 TAMs (Figure 15, below penel). FasL expression in $CD8^+$ T cells increased the most in the triple combination group. This result suggested the presence of FasL-mediated tumor killing by infiltrating T cells.

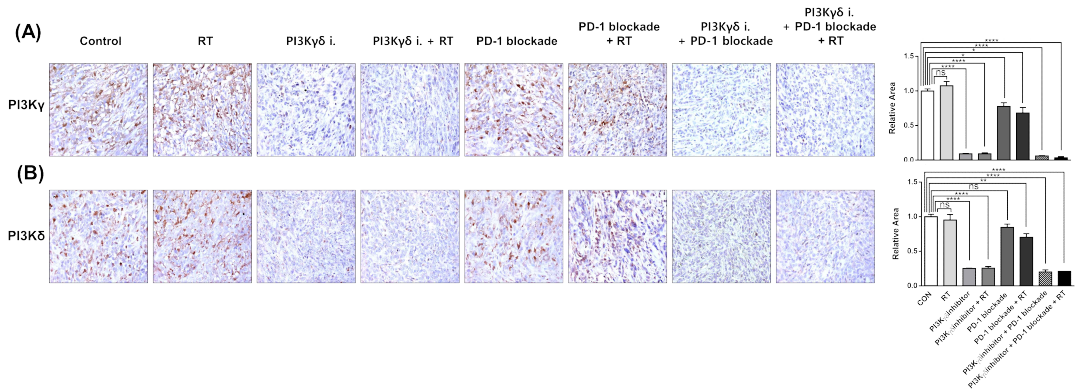

Figure 11. Immunohistochemistry results for PI3Kγ and PI3Kδ expression level in tumor according to treatment group.

The representative micrographs of tumor tissue were presented. The relative area of the stained region based on the control group was quantified in the graph (n=3). These stained sections were observed at 40× magnification using a light microscope. *, $P < 0.05$; **, $P < 0.01$; ****, $P < 0.0001$; ns, not significant. Abbreviations: CON = control; i. = inhibitor; RT = radiation therapy.

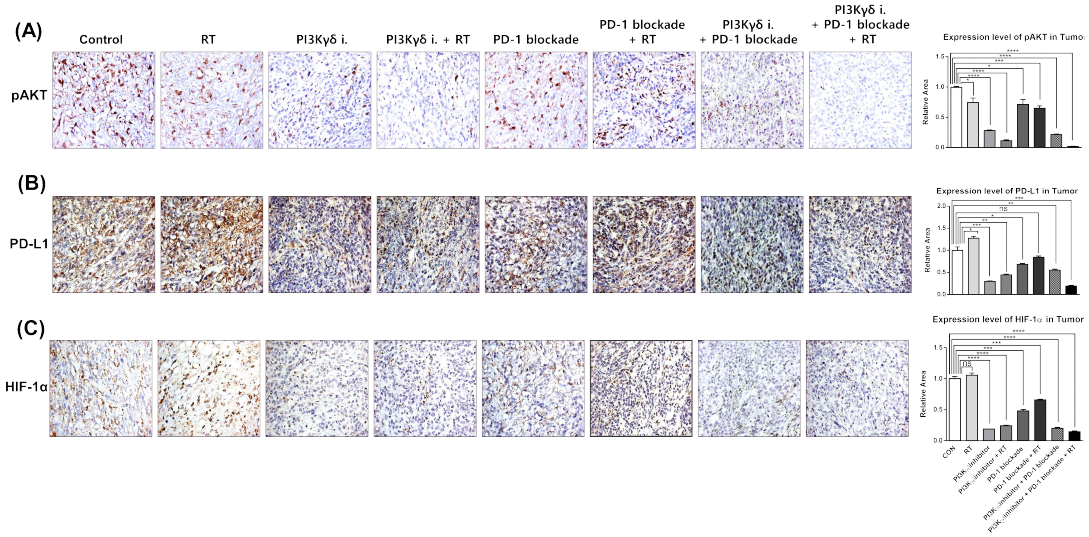

Figure 12. Immunohistochemistry results for pAKT, PD-L1, and HIF-1α expression level in tumor microenvironment according to treatment group.

The representative micrographs of tumor tissue were presented. The relative area of the stained region based on the control group was quantified in the graph (n=3). These stained sections were observed at 40× magnification using a light microscope. *, $P < 0.05$; **, $P < 0.01$; ***, $P < 0.001$; ****, $P < 0.0001$; ns, not significant. Abbreviations: CON = control; i. = inhibitor; RT = radiation therapy.

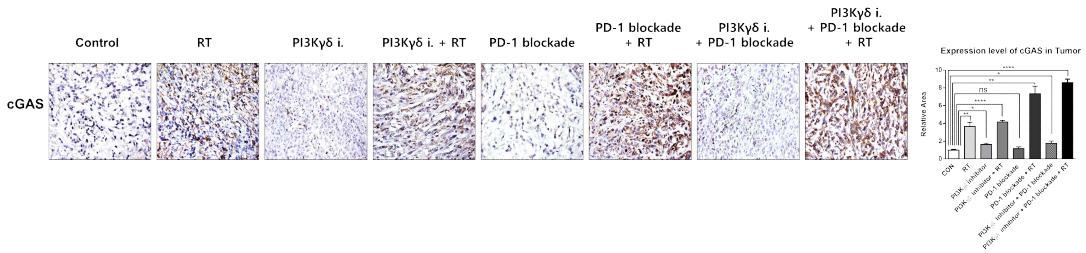

Figure 13. Immunohistochemistry results for cGAS expression level in tumor microenvironment according to treatment group.

The representative micrographs of tumor tissue were presented. The relative area of the stained region based on the control group was quantified in the graph (n=3). These stained sections were observed at 40× magnification using a light microscope. *, $P < 0.05$; **, $P < 0.01$; ****, $P < 0.0001$; ns, not significant. Abbreviations: CON = control; i. = inhibitor; RT = radiation therapy.

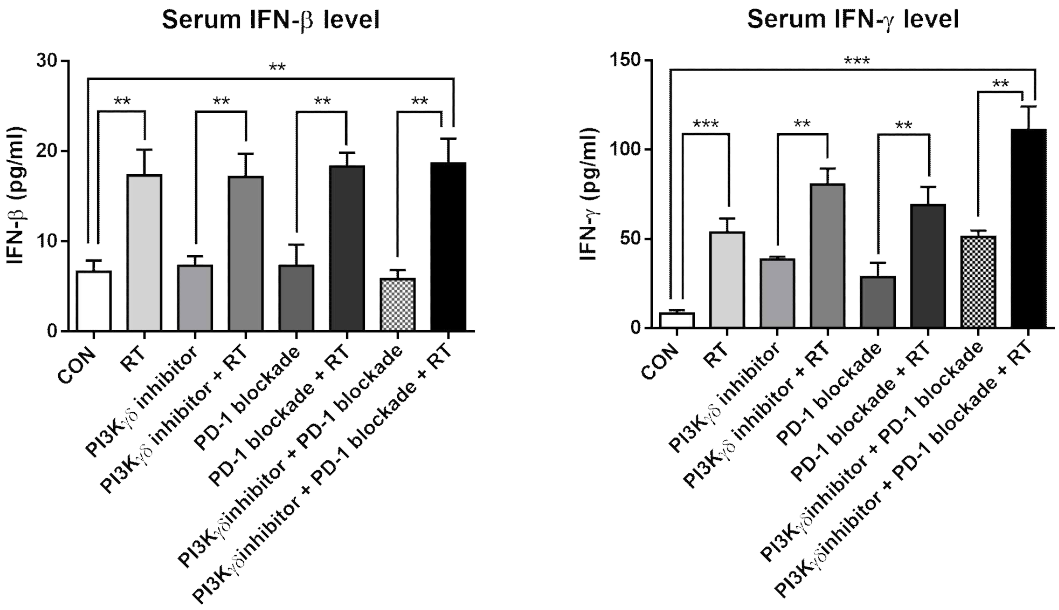

Figure 14. Effects of PI3Kγδ inhibitor and RT on the production of interferons.

The graphs of interferon beta and interferon gamma levels in serum at 1 week after RT was present (n=3). The amount of interferon beta and interferon gamma from each group was quantified in the graph. **, $P < 0.01$; ***, $P < 0.001$. Abbreviations: CON = control; RT = radiation therapy; IFN = interferon.

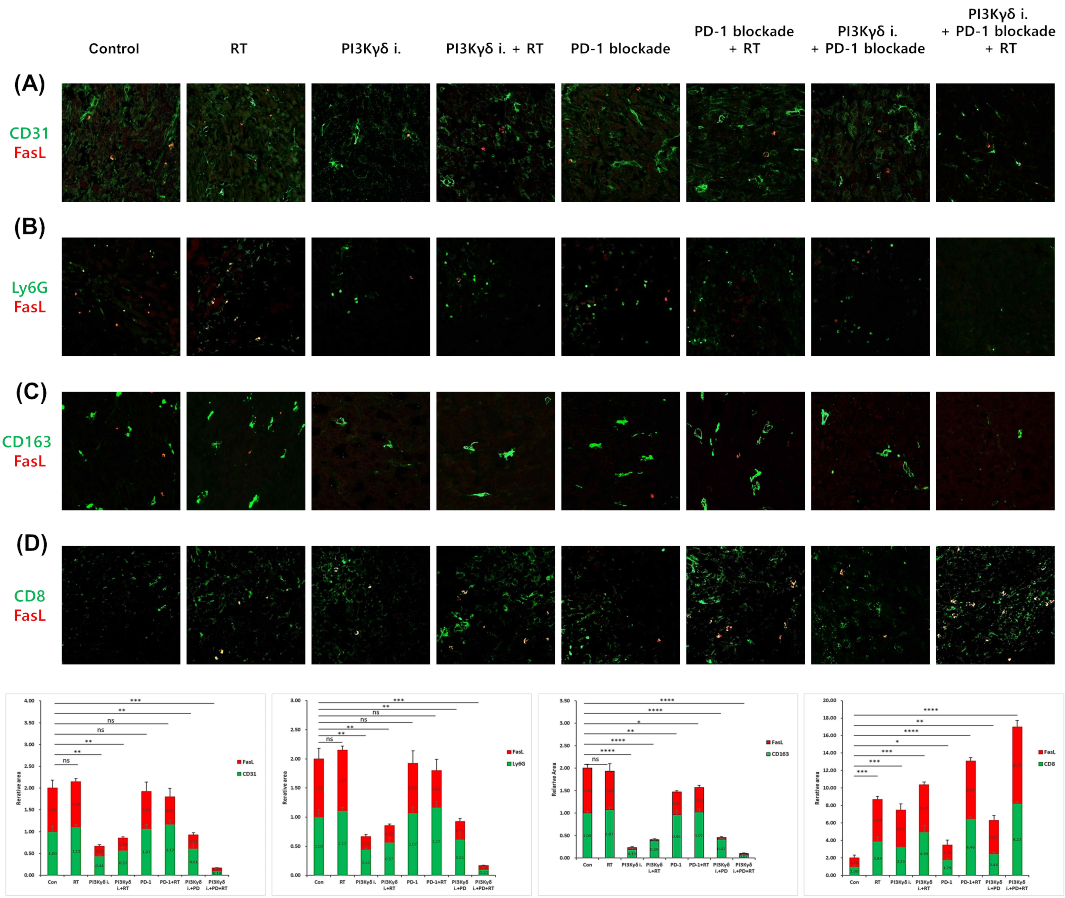

Figure 15. Immunofluorescence staining of Fas-ligand (FasL) expression with endothelial cell marker CD31 (A), PMN-MDSC marker Ly6G (B), TAM marker CD163 (C) and CD8 (D).

The representative immunofluorescence micrographs of tumor tissue were presented and observed at 40× magnification using a confocal microscopy. The fluorescence intensity in the images was quantified in graph. *, $P < 0.05$; **, $P < 0.01$; ***, $P < 0.001$; ****, $P < 0.0001$; ns, not significant. Abbreviations: Con = control; i. = inhibitor; RT = radiation therapy.

4. RT and/or PI3Kγδ inhibitor modulated immune cells in the spleen and dLN

To assess the immune-modulating effect of each treatment, we measured relative proportions of the immune repertoire, including $CD4^+Foxp3^+$ Tregs, $CD11b^+$ $Ly6C^{low}Ly6G^{high}$ PMN-MDSCs, and $CD8^+$ cytotoxic T cells in samples from the 4T1-luc tumor-bearing mice.

In spleen tissue, RT increased $CD8^+$ cytotoxic T cells, immune-suppressive Tregs, and PMN-MDSCs. PI3Kγδ inhibitor lowered Tregs and PMN-MDSCs, achieving significant gains in splenic $CD8^+$ T cells particularly after triple combination therapy. The triple combination group had the lowest mean level of Tregs (Figure 16A). The PMN-MDSC is a predominant type in the immune repertoire in spleen cells of 4T1 tumor-bearing mice. Use of RT alone resulted in increased numbers of PMN-MDSCs. However, mice treated using PI3Kγδ inhibitor alone or a combination that included PI3Kγδ inhibitor had decreased proportions of PMN-MDSCs and PMN-MDSC:M-MDSC ratios (Figure 16B). Uninvolved dLNs from a mouse of each group had a similar immune cell profile (Figure 17A-C). These results indicated that PI3Kγδ inhibitor could suppress PMN-MDSCs in the spleen and the dLNs. In contrast, $CD8^+$ cytotoxic T cells rather than $CD4^+$ T cells increased in all treatment groups (Figure 16C). In particular, the proportion of $CD8^+$ cytotoxic T cells was most elevated when the triple combination therapy was used ($P < 0.0001$).

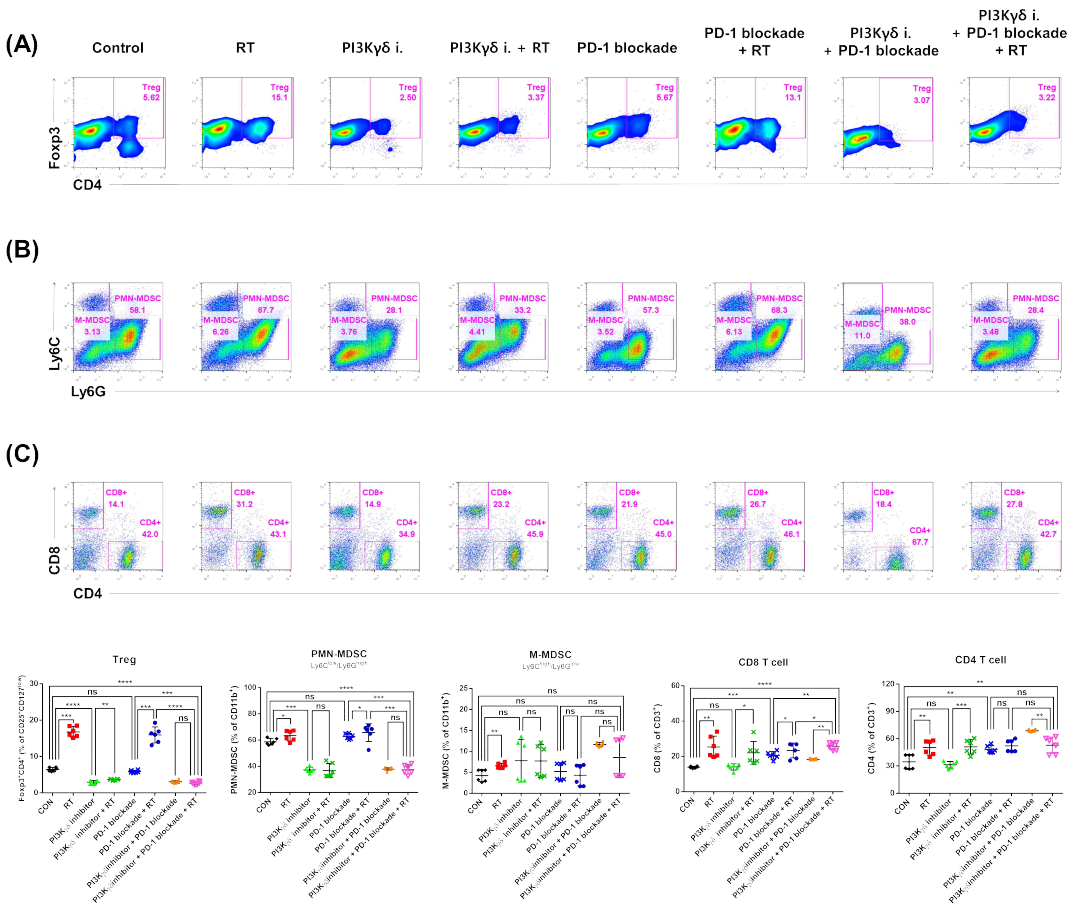

Figure 16. Immune cell profiles in the spleen, in accordance with the treatment group.

Flow cytometric analysis results for Tregs ($CD4^{+}Foxp3^{+}$), PMN-MDSCs ($Ly6C^{low}Ly6G^{high}$) and $CD3^{+}CD8^{+}$ cytotoxic T cells are represented in (A), (B) and (C), respectively. Results of quantification in the spleen are presented in graphs, respectively. *, $P < 0.05$; **, $P < 0.01$; ***, $P < 0.001$; ****, $P < 0.0001$; ns, not significant. Abbreviations: CON = control; i. = inhibitor; M-MDSC = mononuclear myeloid-derived suppressor cell; PMN-MDSC = polymorphonuclear myeloid-derived suppressor cell; RT = radiation therapy; Treg = regulatory T cell.

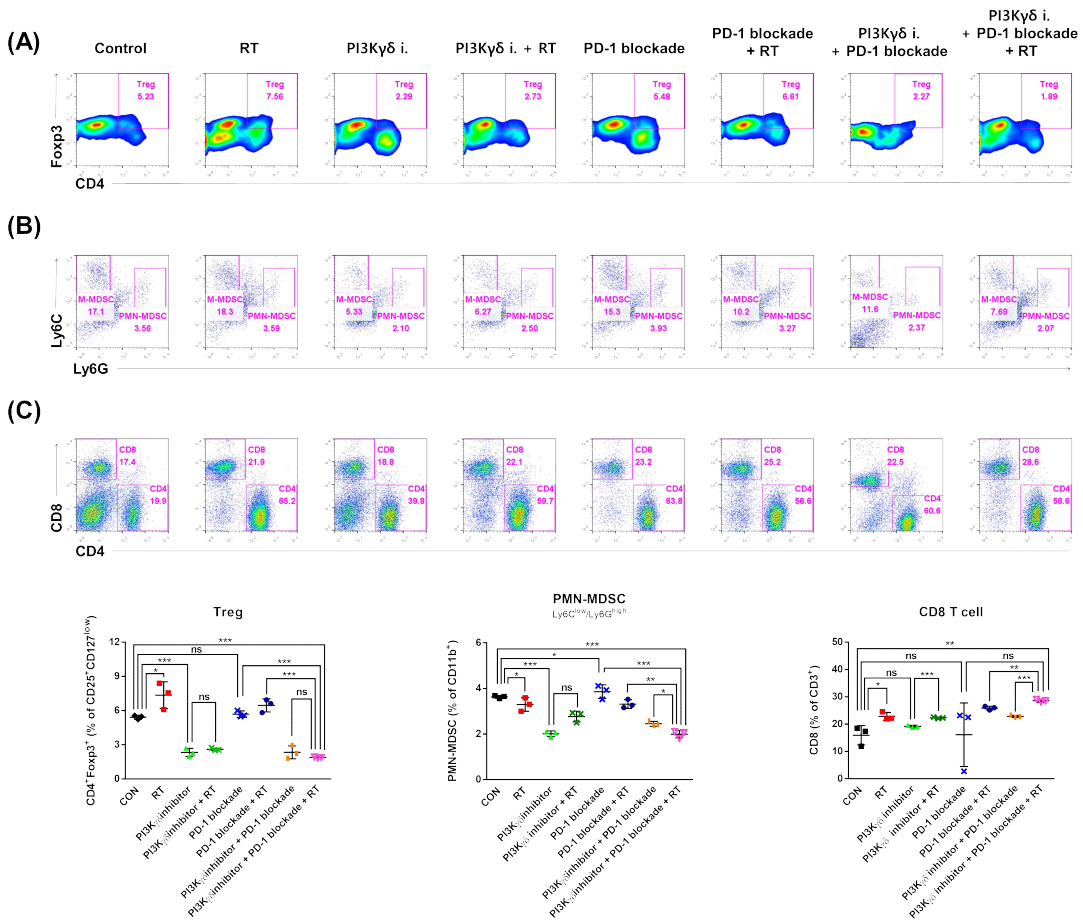

Figure 17. Immune cell profiles in the dLN, in accordance with the treatment group.

Flow cytometric analysis results for Tregs ($CD4^+Foxp3^+$), PMN-MDSCs ($Ly6C^{low}Ly6G^{high}$) and $CD3^+CD8^+$ cytotoxic T cells are represented in (A), (B) and (C), respectively. Results of quantification in the spleen are presented in graphs, respectively. *, $P < 0.05$; **, $P < 0.01$; ***, $P < 0.001$; ns, not significant. Abbreviations: CON = control; i. = inhibitor; PMN-MDSC = polymorphonuclear myeloid-derived suppressor cell; RT = radiation therapy; Treg = regulatory T cell.

5. RT and/or PI3Kγδ inhibitor modulated immune cells in the TME

In the TME, RT induced slight increases in Treg populations but PI3Kγδ inhibitor significantly lowered proportions of Tregs (Figure 18A). The results for MDSCs indicated that RT also increased PMN-MDSCs in the TME but PI3Kγδ inhibitor significantly lowered this population. Use of the triple combination decreased the numbers of PMN-MDSCs the most, as well as the PMN-MDSC:M-MDSC ratio, compared with the other treatment modalities (Figure 18B). RT increased M2 TAMs within the TME; PI3Kγδ inhibitor significantly lowered M2 TAMs. Of all treatments, the triple combination reduced the numbers of M2 TAMs the most, which was driven by the switching of M2 to M1 TAMs (Figure 19A). RT alone slightly elevated the numbers of tumor-infiltrating $CD8^+$ cytotoxic T cells in the TME, which was further increased via combination with PI3K inhibitor or PD-1 blockade. The triple combination group had the highest number of tumor-infiltrating $CD8^+$ cytotoxic T cells in the TME (Figure 19B, $P<0.001$). Except for the RT alone group, the numbers of tumor-infiltrating $CD4^+$ T cells in most groups were not significantly different compared with the control group (Figure 19B). These results were consistent with the accompanying immunohistochemistry results. Taken together, these results suggested that selective inhibition of PI3Kγδ combined with RT can promote an adaptive immune response.

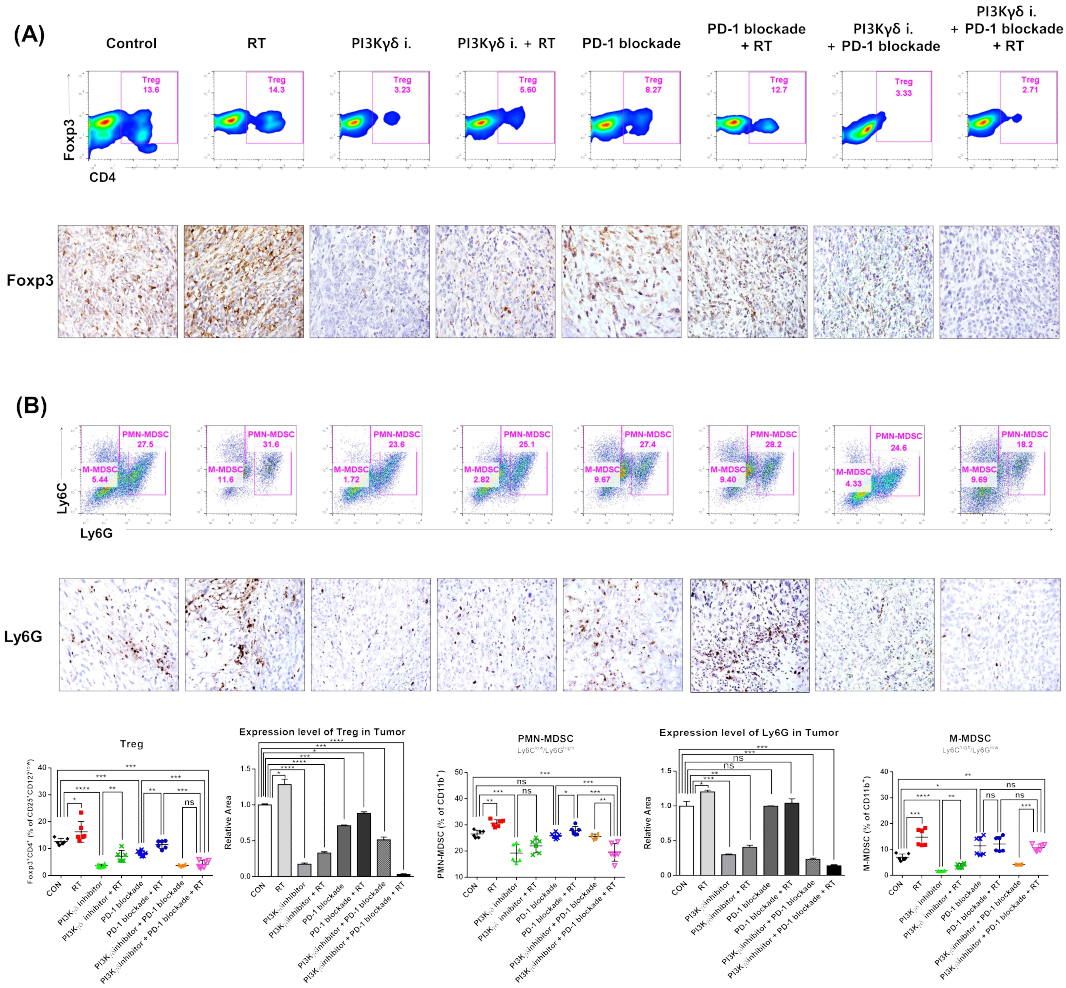

Figure 18. Immune cell profiles of Tregs and MDSCs in the TME, in accordance with the treatment group.

Flow cytometric analysis results for Tregs ($CD4^{+}Foxp3^{+}$) and PMN-MDSCs ($Ly6C^{low}Ly6G^{high}$) are represented in (A) and (B), respectively. Results of quantification in the spleen are presented in graphs, respectively. *, $P < 0.05$; **, $P < 0.01$; ***, $P < 0.001$; ns, not significant. Abbreviations: CON = control; i. = inhibitor; PMN-MDSC = polymorphonuclear myeloid-derived suppressor cell; RT = radiation therapy; Treg = regulatory T cell.

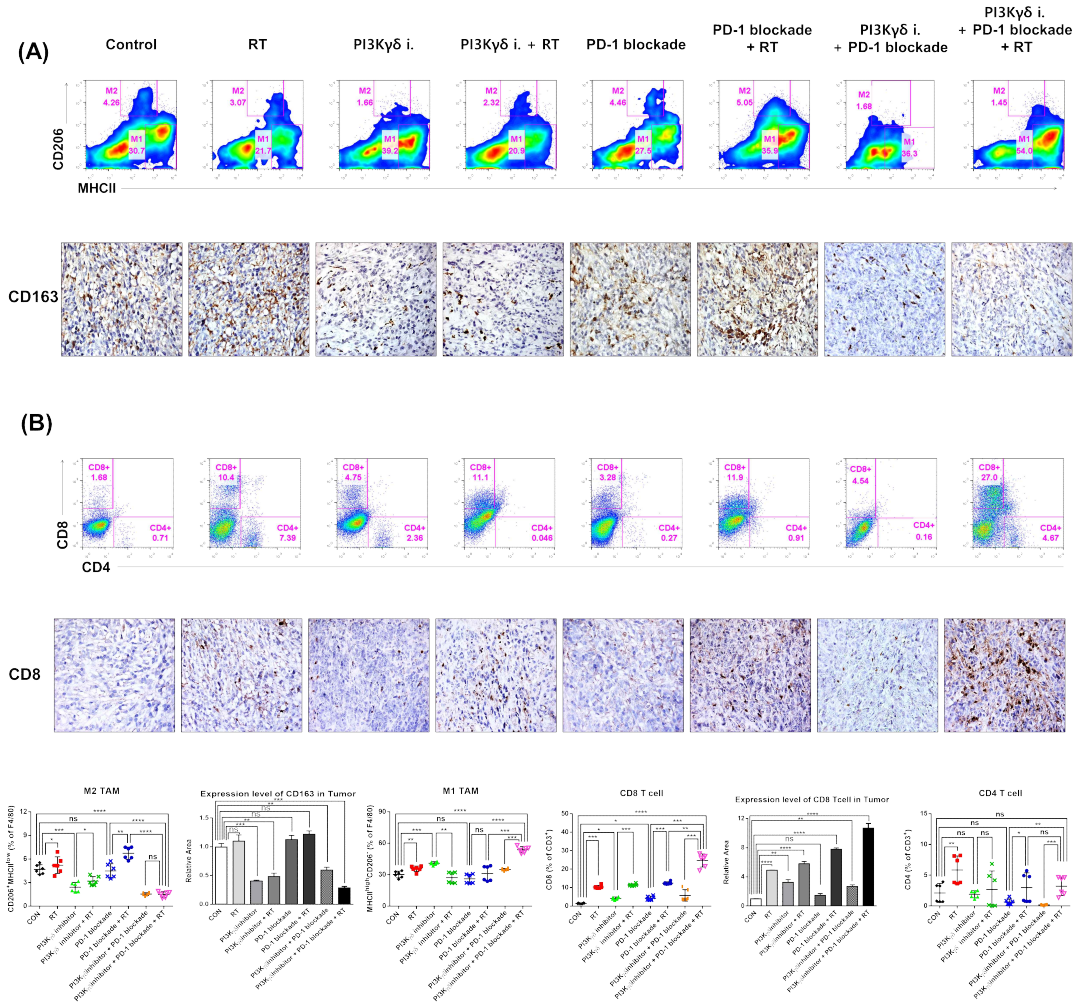

Figure 19. Immune cell profiles of TAMs and $CD8^+$ T cells in the TME, in accordance with the treatment group.

Flow cytometric analysis results for $CD3^+CD8^+$ cytotoxic T cells and TAMs ($CD11b^+F4/80^+$) are represented in (A) and (B), respectively. Results of quantification in the spleen are presented in graphs, respectively. *, $P < 0.05$; **, $P < 0.01$; ***, $P < 0.001$; ns, not significant. Abbreviations: CON = control; i. = inhibitor; RT = radiation therapy; TAM = tumor associated macrophage.

6. Transcriptomic analysis of humanized patient-derived xenograft samples

Humanized mouse-bearing patient-derived xenografts (humanized PDXs) were allocated to one of eight groups: control, RT, PI3Kγδ inhibitor, PI3Kγδ inhibitor + RT, PI3Kγδ inhibitor + PD-1 blockade, PD-1 blockade, PD-1 blockade + RT, or triple combination. The growth curve analysis revealed that the triple combination group showed the most superior anti-tumor effect ($P<0.001$) (Figure 20A). Gross tumor volumes were also the smallest among the other groups (Figure 20B). These results indicated the triple combination had the greatest anti-tumor effect in the humanized PDX model.

We used the CIBERSORTx bioinformatic tool to deconvolute the immune cell repertoire. The results for relative fractions are compared in Figure 21A. Compared with the control group, humanized PDX treated with triple combination therapy showed increased $CD8^+$ T cells. The triple combination group also had the most decreased M2 TAM numbers. As a ratio of immune-suppressive to immune-stimulating cells, the calculated value of (M2 TAM x Treg) / (M1 TAM x CD8 T cells) was the smallest in the triple combination group. The results for relative fractions and calculated values are presented in Table 1.

We investigated canonical gene-signatures related to immune suppressive functions. Sample-wise comparison revealed that most humanized PDX tumors treated with the triple combination had low activity of the vascular endothelial growth factor (VEGF), CXCR4, PD-1, and CTLA4 signaling pathways (Figure 21B). In a group-wise Kyoto Encyclopedia of Genes and Genomes (KEGG) pathway comparison, we computed P-values for respective experimental groups compared with the control group. Compared with the control group,

the triple combination group showed significantly different activities in KEGG pathways, such as cytokine receptor interaction ($P<0.001$), NF-kappa B signaling ($P=0.002$), chemokine signaling ($P=0.002$), Fc gamma receptor-mediated phagocytosis ($P=0.0049$), and the phospholipase D signaling pathway ($P=0.008$) (Figure 21C).

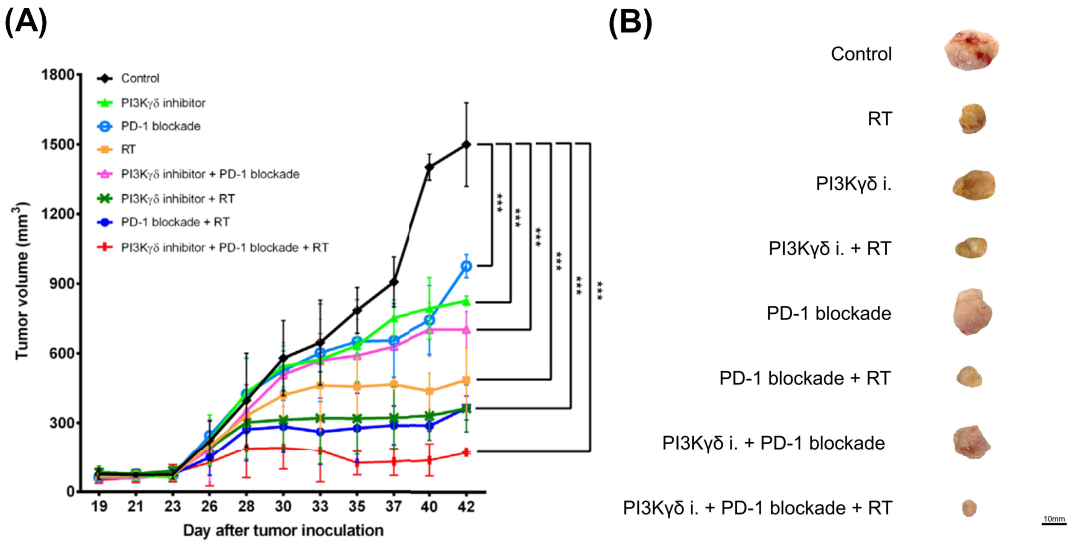

Figure 20. Comparison of tumor growth results for humanized PDX model, according to treatment group.

(a) Tumor growth curves according to treatment group. (b) Comparison of humanized PDX gross tumor samples, according to treatment group. Scale bars = 10 mm. ***, P < 0.001. Abbreviations: i. = inhibitor; RT = radiation therapy.

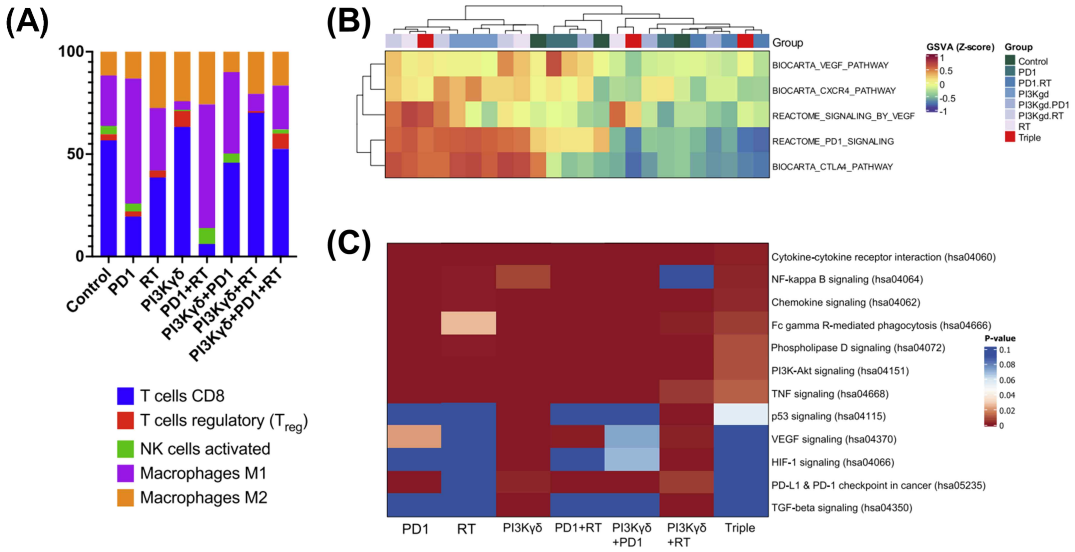

Figure 21. Comparison of RNA sequencing results for humanized PDX model, according to treatment group.

(A) Comparison of relative fractions derived using CIBERSORTx deconvolution algorithm. (B) Canonical pathways presented as scaled GSVA score are compared. (C) Compared to control group, differential KEGG pathway results are shown. Abbreviations: GSVA = gene set variation analysis; NK = natural killer; PD1 = PD-1 blockade; RT = radiation therapy; PI3Kγδ = PI3Kγδ inhibitor; Triple = triple combination.

	Control	PI3Kgd	RT	PD1	PI3Kgd+RT	PD1+RT	PI3Kgd+PD1	PI3Kgd+PD1+RT
B cells naive	0.026123	0.047043	0.057944	0.102811	0.034351	0	0.006737	0.004098
B cells memory	0	0	0	0	0	0.019902	0	0
Plasma cells	0.024776	0.006384	0	0.068225	0	0.074894	0.069081	0.011612
T cells CD8	0.033255	0.088291	0.013531	0	0.038566	0	0.045386	0.107502
T cells CD4 naive	0	0	0	0	0	0	0	0
T cells CD4 memory resting	0.408794	0.274698	0.367065	0.165808	0.326952	0.247338	0.161096	0.191042
T cells CD4 memory activated	0.033316	0	0.062007	0.044956	0.013966	0.017973	0.091015	0.01859
T cells follicular helper	0.088697	0.12035	0.053789	0.150745	0.078211	0.02398	0.116791	0.102694
T cells regulatory (Tregs)	0	0.070856	0	0	0.007029	0	0	0.03322
T cells gamma delta	0	0	0	0	0	0	0	0
NK cells resting	0.192295	0.185802	0.200134	0.064414	0.217507	0.002179	0.131094	0.114041
NK cells activated	0.001084	0	0	0	0	0.026511	0.010187	0.013059
Monocytes	0.031572	0.016831	0.028195	0	0.02791	0	0	0.028389
Macrophages M0	0.024509	0.059968	0.125305	0.139353	0.102558	0.283148	0.155276	0.208371
Macrophages M1	0.054348	0.016615	0.05338	0.189808	0.051834	0.189635	0.14767	0.065858
Macrophages M2	0.013014	0.078639	0.02832	0.015535	0.038366	0.042461	0	0.012163
Dendritic cells resting	0.003999	0.007641	0	0	0.016495	0	0	0
Dendritic cells activated	0.011488	0	0.010296	0.010176	0	0.004715	0.00909	0
Mast cells resting	0.052732	0.026841	0	0.048168	0.046255	0.067264	0.056578	0.08936
Mast cells activated	0	0	0	0	0	0	0	0
Eosinophils	0	0	0	0	0	0	0	0
Neutrophils	0	0	0	0	0	0	0	0
M2 / M1 Ratio	0.239457	4.733012	0.530536	0.081846	0.740170544	0.223909089	0	0.184685232
Tregs / CD8 Ratio	0	0.588749	0	0	0.089872269	0	0	0.323485306
M2 x Tregs / M1 x CD8	0	2.786559	0	0	0.066520806	0	0	0.059742959

Table 1. The CIBERSORTx deconvoluted immune cells from humanized PDX samples.

The list of immune cell repertoires and calculated values were derived using the CIBERSORTx deconvolution algorithm from RNA-sequencing data. Abbreviations: NK = natural killer; PD1 = PD-1 blockade; RT = radiation therapy; PI3Kgd = PI3Kγδ inhibitor; Tregs = regulatory T cells.

7. Immune cell proportions of TME in The Cancer Genome Atlas pan-cancer cohort

Using each median cutoff value for *CD274*, *PIK3CG*, and *PIK3CD* mRNA expression, 5,534 patients were grouped into the high expression group, and 5,535 patients were allocated to the low expression group. Samples with high $CD8^+$ T cell infiltration were enriched in *PD-L1*, *PIK3CG*, and *PIK3CD* (Figure 22). Mean fractions of immune cells were positively correlated with immune score, and samples with high immune scores were clustered into the *PD-L1*, *PIK3CG*, and *PIK3CD* high expression groups. We verified that there were statistically significant differences between immune cell fractions (one-sample t-test <0.001, Table 2). Median fractions of deconvoluted immune cells, including $CD8^+$ T cells, M1 TAMs, M2 TAMs, and Tregs, were increased in the *PIK3CG* high expression group (Figure 23A, Wilcoxon rank test, P<0.001). This trend was also found in the *PIK3CD* high expression group (Figure 23B, P<0.001), except for the Treg fractions (P=0.147). Consistent with this result, the *PIK3CG* and the *PIK3CD* high expression groups had higher immune scores than the low expression groups (Table 3). After inversely weighting immune scores, we calculated the adjusted Treg/$CD8^+$ T cell and M2/M1 TAM ratios. As a result, we found higher Treg/$CD8^+$ T ratios in the *PIK3CG* and *PIK3CD* high expression groups, compared to the low expression groups. The results for the M2/M1 ratios revealed a similar trend.

A total of 10,844 patients with available overall survival (OS) data were collected to compare survival between expression groups. The *PIK3CG* high expression group had an inferior OS rate, compared with the low expression group (Figure 24A, 5-year: 61.2% vs. 58.6%, respectively, log-rank test, P=0.002). We also found a worse OS in

the *PIK3CD* high expression group compared with the low expression group (Figure 24B, 5-year: 62.7% vs. 57.3%, respectively, log-rank test $P<0.001$).

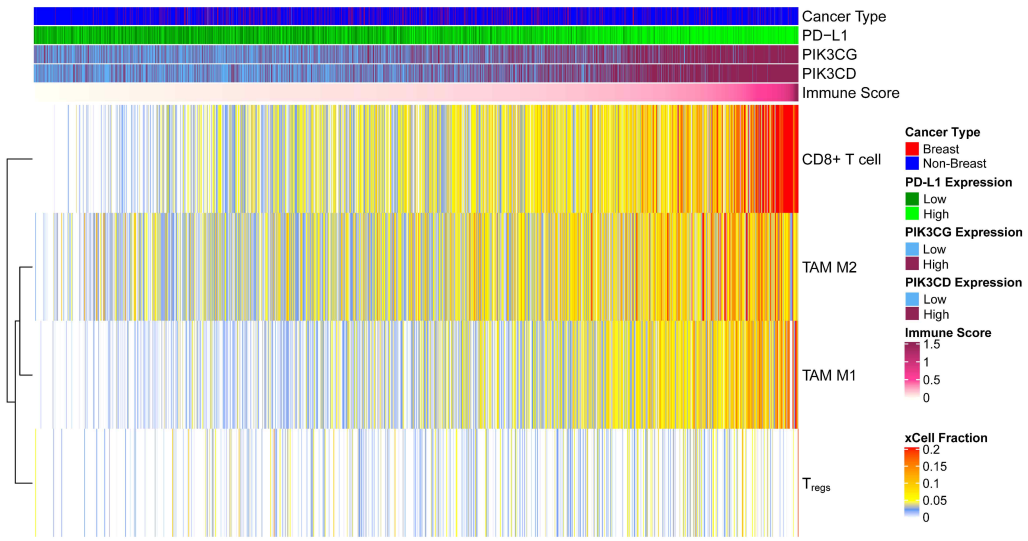

Figure 22. Heatmap representing immune cell fractions derived from xCell deconvolution algorithm according to TCGA breast cancer patient samples.

The x-axis indicates each sample and the y-axis shows four immune cell types. Abbreviations: PD-L1 = programmed death-ligand 1; PIK3CD = phosphatidylinositol-4,5-bisphosphate 3-kinase catalytic subunit delta; PIK3CG = phosphatidylinositol-4,5-bisphosphate 3-kinase catalytic subunit gamma; TAM = tumor associated macrophage; TCGA = The Cancer Genome Atlas.

Cell Type	PIK3CG Expression	Actual Mean	95% CI	P-value (Mean=0)	PIK3CD Expression	Actual Mean	95% CI	P-value (Mean=0)
CD8+ T cells	Low	0.037	0.036-0.038	<0.001	Low	0.033	0.032-0.033	<0.001
	High	0.078	0.075-0.081	<0.001	High	0.082	0.080-0.085	<0.001
M1 TAM	Low	0.019	0.018-0.019	<0.001	Low	0.019	0.018-0.019	<0.001
	High	0.045	0.044-0.046	<0.001	High	0.045	0.044-0.046	<0.001
M2 TAM	Low	0.040	0.039-0.041	<0.001	Low	0.039	0.038-0.040	<0.001
	High	0.060	0.058-0.061	<0.001	High	0.061	0.060-0.063	<0.001
T_{reg}	Low	0.005	0.005-0.006	<0.001	Low	0.007	0.007-0.008	<0.001
	High	0.010	0.009-0.010	<0.001	High	0.008	0.007-0.008	<0.001

Table 2. The xCell deconvoluted cells in TCGA pan cancer cohort.

The actual mean and statistical values were obtained from significant differences between various immune cell fractions based on the low or high target gene expression levels. Abbreviations: CI = Confidence Interval; PIK3CG = phosphatidylinositol-4,5-bisphosphate 3-kinase catalytic subunit gamma; PIK3CD = phosphatidylinositol-4,5-bisphosphate 3-kinase catalytic subunit delta; TAM = tumor associated macrophage; TCGA = The Cancer Genome Atlas.

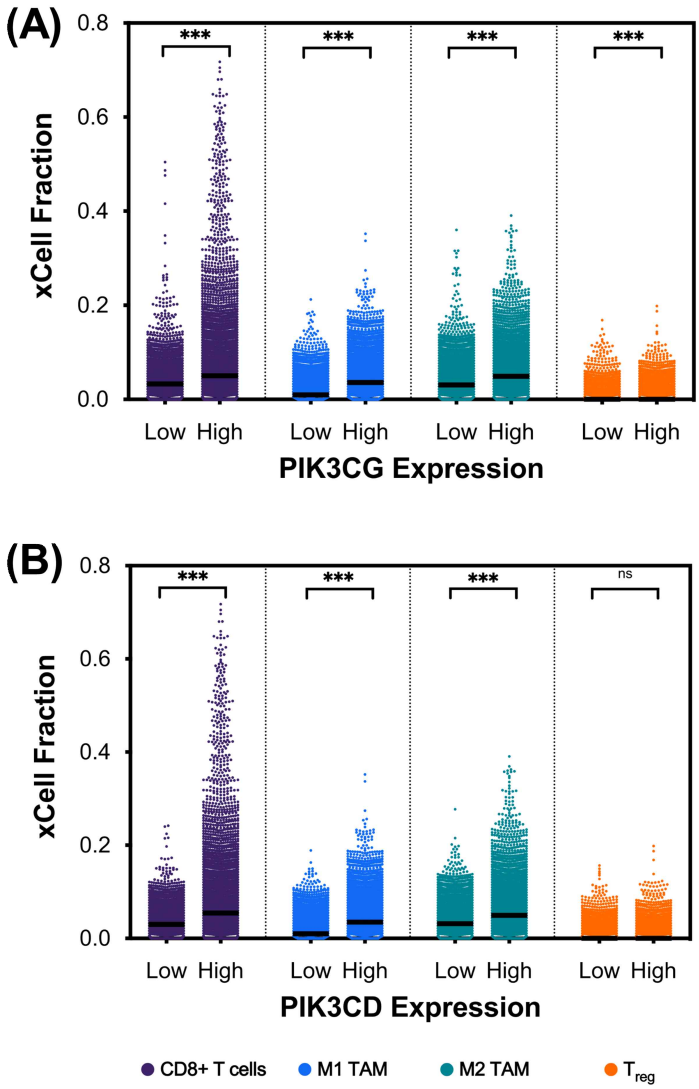

Figure 23. Scatter bar plot of immune cell fractions in accordance with *PIK3CG* high and low expression groups (A) and *PIK3CD* high and low expression groups (B).

Each dot represents a deconvoluted immune cell. Black bars represent median fractions of immune cells in the group. Wilcoxon rank-sum tests were performed to compare median fractions of immune cells between high versus low expression groups. ***, $P < 0.001$; ns, not significant. Abbreviations: PIK3CD = phosphatidylinositol-4,5-bisphosphate 3-kinase catalytic subunit delta; PIK3CG = phosphatidylinositol-4,5-bisphosphate 3-kinase catalytic subunit gamma; TAM = tumor associated macrophage.

	PIK3CG Expression				*PIK3CD* Expression			
	Low		High		Low		High	
Mean Ratio	Unadjusted	Adjusted	Unadjusted	Adjusted	Unadjusted	Adjusted	Unadjusted	Adjusted
T_{reg}/CD8+	0.135	0.027	0.128	0.050	0.212	0.022	0.098	0.026
M2/M1 TAMs	2.105	0.424	1.333	0.516	2.053	0.212	1.350	0.353
Mean Immune Score	0.201		0.387		0.103		0.262	

Table 3. Unadjusted and Adjusted mean immune-suppressive/immune-stimulating immune cell ratio according to the *PIK3CG* or *PIK3CD* mRNA expression groups.

The inversely weighting immune scores were calculated by the adjusted Treg/CD8+ T cell and M2/M1 TAM ratios. The adjusted ratio was calculated by the inverse-weighting mean immune score to the unadjusted ratio. Abbreviations: PIK3CG = phosphatidylinositol-4,5-bisphosphate 3-kinase catalytic subunit gamma; PIK3CD = phosphatidylinositol-4,5-bisphosphate 3-kinase catalytic subunit delta; TAMs = tumor associated macrophages; Treg = regulatory T cells; .

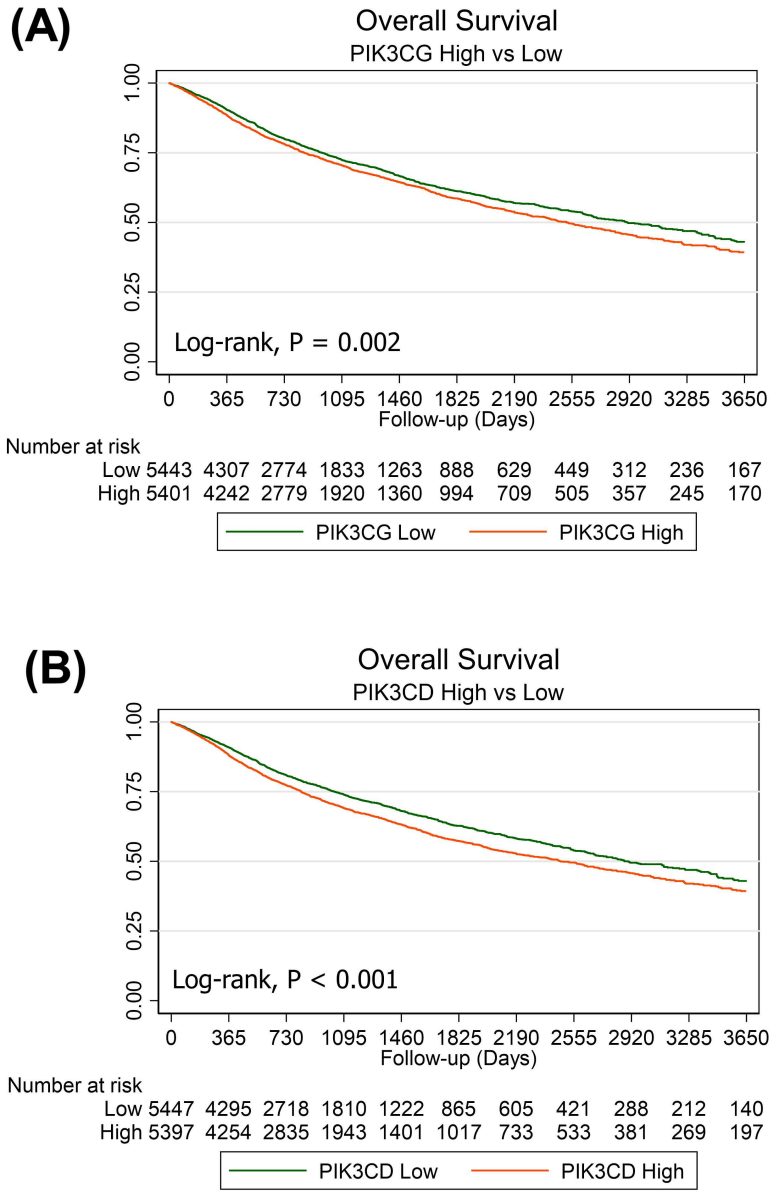

Figure 24. Comparing immune cell population and overall survival between *PIK3CD* or *PIK3CG* expression groups.

(A) KaplaneMeier curves for overall survival according to *PIK3CG* expression groups and (B) *PIK3CD* expression groups. Log-rank tests were performed, and p-values are presented within graphs. Abbreviations: PIK3CD = phosphatidylinositol-4,5-bisphosphate 3-kinase catalytic subunit delta; PIK3CG = phosphatidylinositol-4,5-bisphosphate 3-kinase catalytic subunit gamma;.

IV. Discussion

This study found enhanced anti-tumor effects of PI3Kγδ inhibitor when combined with PD-1 inhibitor and RT in 4TI TNBC mouse and humanized PDX models [23]. The study findings included decreased tumor volume of the non-irradiated tumors. These local and distant anti-tumor effects were mediated by modulation of the immune cell repertoire. The humanized PDX model revealed that tumors treated using triple combination therapy had differential immune-related signatures. We also assessed the TME according to *PIK3CG* and *PIK3CD* gene expression in The Cancer Genome Atlas (TCGA) pan-cancer cohort. The *PIK3CG* or *PIK3CD* high expression groups had increased ratios of immune-suppressive/immune-stimulating cells and significantly inferior OS rates.

Although ICB use results in durable responses, patients often experience disease progression. Hyperprogression is a dramatic example of ICB resistance and is defined as more than two times accelerated tumor growth rate, even when ICBs are used [39]. We found a trend similar to that of hyperprogression in the mice treated with PD-1 blockade alone. After 35 days from tumor inoculation, the growth rates accelerated and tumor sizes eventually even exceeded the sizes of the control group tumors. As expected, these mice had the worst survival. Underlying mechanisms of hyperprogression and predictive biomarkers remain to be elucidated. However, they can be explained, in part, by the immunosuppressive TME led by Treg expansion, $CD8^+$ cytotoxic T cell depletion, and the polarization into M2 TAMs or MDSCs [40]. Our study found that PD-1 blockade alone had no effect on the PMN-MDSC and M2 TAM populations in the TME [23]. The actions of PI3Kδ and PI3Kγ inhibitors against

immune-suppressive cells have been shown by other studies. For example, PI3Kδ inhibitor promotes anti-tumor immune effect via inhibition of Tregs and possibly PMN-MDSCs, subsequently promoting $CD8^+$ T cell functions [17, 26]. When combined with PD-1 blockade, PI3Kγ inhibitor activates memory T cells and enhances recruitment of $CD8^+$ cytotoxic T cells by blocking PI3Kγ signaling within TAMs [41]. Han et al. [23] and Henau et al. [27] found that PI3Kγ inhibition switched the activation of macrophages from an immunosuppressive M2-like phenotype to a more inflammatory M1-like one. We also observed a significant decrease in M2 TAMs with an increase in M1 TAMs, particularly when PI3Kγδ inhibitor was combined. Given that switching of polarization within TAMs is possible [8], PI3Kγδ inhibitor may contribute to a shift from M2 toward M1 TAMs within the TME.

Another strategy to overcome ICB resistance is to convert the immunologically “cold” tumor to a “hot” tumor [42]. Treg depletion induced by ICB alone is not sufficient to induce an anti-tumor response in “cold” tumors [43]. To develop “hot” tumors, a few preclinical studies found that local high-dose RT can promote $CD8^+$ cytotoxic T cell infiltration into the TME [44], implicating RT-induced immunogenic cell death [21,45]. RT can initiate type I IFN production in the TME and release tumor-associated antigens via activation of the cGAS/STING pathway [21]. Its activation is necessary for an RT-induced *in situ* tumor vaccination effect. Tumor-associated antigens are recognized by antigen-presenting cells and presented to T cells that can reject tumor cells locally and systemically [46]. In this current study, the cGAS level in the TME was elevated using RT alone or RT combined with either PD-1 blockade or PI3Kγδ inhibitor. The triple combination group had the

most upregulated cGAS expression. This phenomenon depends on the dose/fraction schedule [47-49]. Of the various RT regimens, the hypofractionated RT we used in this study elicits the abscopal effect. This hypofractionated RT regimen effectively induced increased serum IFNβ and IFNɣ. IFNβ is the prerequisite for the *in situ* vaccination effect via RT [47]; IFNɣ is essential for tumor rejection by $CD8^+$ cytotoxic T cells in the murine model [50]. Previous studies [48,49] found that the elevated IFNβ and IFNɣ following hypofractionated RT mediate the abscopal effect in the murine model. Thus, the hypofractionated regimen we used in this study seemed to activate the STING pathway via upregulation of cGAS expression and to increase serum IFNβ and IFNɣ levels for the adaptive immune response.

RT increases immune-suppressive features, such as M2 TAMs [51] and Tregs, [43] in the TME. We found an increase in M2 TAMs within the TME using RT or RT + PD-1 blockade, except when combined with the PI3Kɣδ inhibitor. The RT alone group had significantly increased splenic Tregs and PMN-MDSCs, compared with the control group. This result suggested there was a limited abscopal effect using RT alone. However, we found decreased Tregs and PMN-MDSCs and increased $CD8^+$ cytotoxic T cells in spleen cells following triple combination therapy, suppressing growth of non-irradiated tumors. This abscopal effect was verified in luciferase-untagged 4TI tumors while it did not occur in immune-compromised nude mice.

PIK3CD and *PIK3CG* genes are generally overexpressed in solid tumors [52]. However, there have been no reports of studies that investigated the relationship between *PIK3CD/PIK3CG* expression in the TME and OS in patients with cancer. In this study, we found

that the *PIK3CD* and *PIK3CG* high expression group had inferior OS vs. the pan-cancer cohort. To compare the TME between the *PIK3CD* or *PIK3CG* high versus low expression groups, we estimated ratios of immune-suppressive/immune-stimulating cells. Although the TCGA consortium recommends a tumor purity threshold of 60% in tumor samples, there are variations between samples and between cancer types [53]. Samples with low tumor purity (high immune score) had more immune cells that expressed *PIK3CD* and *PIK3CG* mRNA in the heatmap result. Thus, we adjusted tumor purity using the immune score, which is negatively correlated with tumor purity in the TCGA-pan cancer cohort [35]. As couldn't find the significant difference of overall according to high vs. low PI3K gamma or delta expression in breast cancer patients data sets, pan cancer data sets were analyzed. As a result, immune-suppressive cells such as M2 TAMs or Tregs were dominant in the *PIK3CD* and *PIK3CG* high expression group compared to the low expression group. High expression of *PIK3CD* and *PIK3CG* in the TME may contribute to suppression of immunologic cancer cell death and be linked to poor OS. Given the immune modulating effects of using PI3Kγδ inhibitor in this preclinical study, this drug could be tested on solid tumors with immunosuppressive TMEs in clinical trial settings.

The limitation of our study was the absence of validating the results of transcriptome analysis. Further studies would reveal much clearer mechanism through demonstrating the pathways that were found to be significant from the transcriptomic analysis by *in vivo* experiment. In phase 3 clinical trials of PI3Kγδ inhibitor currently in progress, it is administered to patients at a dose of 25 mg by mouth twice daily because the inhibitory constant (Ki) value of the PI3Kγδ inhibitor is considerably low [54]. It was initially intended to

administer the PI3Kγδ inhibitor to mice twice daily in the same manner as to humans; but, the body-weight reduction of mice was severe due to the toxicity of frequent drug administration. Therefore, a high dose (15 mg/kg) of PI3Kγδ inhibitor every other day was the best strategy to administer in order to overcome the low Ki of the inhibitor. The similar previous study has shown that this dose is available for *in vivo* murine model [55]. In this experiment, RT of 8 Gy per fraction in the same manner as stereotactic ablative RT (SABR) was combined with PI3Kγδ inhibitor and PD-1 blockade to demonstrate the *in situ* vaccination effect along with abscopal effect in syngenic and humanized triple-negative breast cancer model. Although this treatment scheme is promising and gaining attention in the field of immunotherapy, there still exists a lack of evidence in clinical and preclinical to apply it to early-stage breast cancer. Instead, recurrent or metastatic settings would be more sufficient to anticipate *in situ* vaccination and abscopal effect from the RT.

This study is the first evidence to show the efficacy of the triple-combination therapy with RT, PI3Kγδ inhibitor, and PD-1 blockade; therefore, it is unclear whether this combination of three treatments is safe. FDA approved clinical trials have examined the use of PI3Kγδ inhibitor for the treatments of chronic lymphocytic leukemia (CLL) or small lymphocytic lymphoma (SLL) regarding its toxicity. The adverse events commonly reported were infections, diarrhea or colitis, and pneumonitis [56]. The ongoing clinical trials of PI3Kγδ inhibitor with a combination of various treatments have firmly addressed the toxicity profiles in humans [54, 57]. Despite several side effects of these PI3Kγδ inhibitors, it is clear that PI3Kγδ inhibitors have significant potential to apply to solid tumors including breast cancer as well as FDA-approved leukemia. Further studies

would be necessary to evaluate the safety of the triple-combination therapy before this regimen could be implemented in clinical settings.

A PI3Kγδ inhibitor, PD-1 blockade, and RT used in combination had superior anti-tumor efficacy, a durable response, and an abscopal effect without severe toxicity in a syngenic 4TI murine tumor model. The immune-modulating effect was identified in the TME, spleen, and dLNs when the trimodal modality was used. The humanized PDX model revealed that tumors treated using the triple combination therapy had favorable features for antitumor immune effect. In human pan-cancer TCGA samples, inferior survival and an immunosuppressive TME were found in the *PIK3CG* or *PIK3CD* high expression groups. A combinational strategy using a selective inhibitor of PI3Kγδ, PD-1 blockade, and RT could be a viable approach to overcome therapeutic resistance of immune checkpoint blockade in patients with immunologically “cold” tumors.

References

1. Robert C, Ribas A, Hamid O, Daud A, Wolchok JD, Joshua AM, et al. Durable complete response after discontinuation of pembrolizumab in patients with metastatic melanoma. J Clin Oncol 2018;36:1668e74.
2. Socinski MA, Jotte RM, Cappuzzo F, Orlandi F, Stroyakovskiy D, Nogami N, et al. Atezolizumab for first-line treatment of metastatic nonsquamous NSCLC. N Engl J Med 2018;378:2288e301.
3. Brooks ED, Chang JY. Time to abandon single-site irradiation for inducing abscopal effects. Nat Rev Clin Oncol 2019;16: 123e35. https://doi.org/10.1038/s41571-018-0119-7.
4. Dirix LY, Takacs I, Jerusalem G, et al. Avelumab, an anti-PD-L1 antibody, in patients with locally advanced or metastatic breast cancer: A phase 1b JAVELIN solid tumor study. Breast Cancer Res Treat 2018;167:671-686.
5. Adams S, Loi S, Toppmeyer D, et al. Pembrolizumab monotherapy for previously untreated, PD-L1-positive, metastatic triple-negative breast cancer: Cohort B of the phase II KEYNOTE-086 study. Ann Oncol 2019;30:405-411.
6. Bos PD, Plitas G, Rudra D, Lee SY, Rudensky AY. Transient regulatory T cell ablation deters oncogene-driven breast cancer and enhances radiotherapy. J Exp Med 2013;210:2435e66. https: //doi.org/10.1084/jem.20130762.
7. Cassetta L, Kitamura T. Macrophage targeting: opening new possibilities for cancer immunotherapy. Immunology 2018;155: 285e93. https://doi.org/10.1111/imm.12976.
8. Fleming V, Groth C, Altevogt P, Umansky V, Nagibin V, Weber R, et al. Targeting myeloid-derived suppressor cells to bypass tumour-induced immunosuppression. Front Immunol 2018;9. https://doi.org/10.3389/fimmu.2018.00398.
9. Kim IS, Gao Y, Welte T, et al. Immuno-subtyping of breast cancer reveals distinct myeloid cell profiles and immunotherapy resistance mechanisms. Nat Cell Biol 2019;21:1113-1126.

10. Tumeh PC, Harview CL, Yearley JH, Shintaku IP, Taylor EJM, Robert L, et al. PD-1 blockade induces responses by inhibiting adaptive immune resistance. Nature 2014;515:568e71. https://doi.org/10.1038/nature13954.
11. Andrews MC, Wargo JA. Immunotherapy resistance: the answers lie ahead – not in front – of us. J Immunother Cancer 2017;5. https://doi.org/10.1186/s40425-017-0212-y.
12. Sharma P, Allison JP. The future of immune checkpoint therapy. Science 2015;348:56e61. https://doi.org/10.1126/science.aaa8172.
13. Vonderheide RH, Domchek SM, Clark AS. Immunotherapy for breast cancer: what are we missing? Clin Canc Res 2017;23: 2640e6. https://doi.org/10.1158/1078-0432.CCR-16-2569.
14. Dewan MZ, Galloway AE, Kawashima N, Dewyngaert JK, Babb JS, Formenti SC, et al. Fractionated but not single-dose radiotherapy induces an immune-mediated abscopal effect when combined with anti-CTLA-4 antibody. Clin Canc Res 2009;15: 5379e88. https://doi.org/10.1158/1078-0432.CCR-09-0265.
15. Demaria S, Kawashima N, Yang AM, Devitt ML, Babb JS, Allison JP, et al. Immune-mediated inhibition of metastases after treatment with local radiation and CTLA-4 blockade in a mouse model of breast cancer. Clin Canc Res 2005;11:728e34.
16. Herrera FG, Bourhis J, Coukos G. Radiotherapy combination opportunities leveraging immunity for the next oncology practice. CA Cancer J Clin 2017;67:65e85. https://doi.org/10.3322/caac.21358.
17. Chang, W. I., Han, M. G., Kang, M. H., Park, J. M., Kim, E. E., Bae, J., Ahn, S. & Kim, I. A. PI3Kαδ Inhibitor Combined With Radiation Enhances the Antitumor Immune Effect of Anti-PD1 in a Syngeneic Murine Triple-Negative Breast Cancer Model. Int J Radiat Oncol Biol Phys. 2021; 110(3): 845 - 58.
18. Koo T, Kim IA. Radiotherapy and immune checkpoint blockades: A snapshot in 2016. Radiat Oncol J 2016;34:250-259.
19. Krysko DV, Garg AD, Kaczmarek A, et al. Immunogenic cell death and DAMPs in cancer therapy. Nat Rev Cancer 2012;12:860-875.
20. Galluzzi L, Buque´ A, Kepp O, et al. Immunogenic cell death in cancer and infectious disease. Nat Rev Immunol 2017;17:97-111.

21. Weichselbaum RR, Liang H, Deng L, Fu Y-X. Radiotherapy and immunotherapy: a beneficial liaison? Nat Rev Clin Oncol 2017;14: 365e79. https://doi.org/10.1038/nrclinonc.2016.211.
22. Wang X, Ding J, Meng LH. PI3K isoform-selective inhibitors: next-generation targeted cancer therapies. Acta Pharmacol Sin 2015;36:1170e6. https://doi.org/10.1038/aps.2015.71.
23. Han, M. G., Jang, B. S., Kang, M. H., Na, D. & Kim, I. A. PI3Kγδ inhibitor plus radiation enhances the antitumour immune effect of PD-1 blockade in syngenic murine breast cancer and humanised patient-derived xenograft model. European Journal of Cancer. 2021; 157: 450-463.
24. Okkenhaug K, Bilancio A, Farjot G, et al. Impaired B and T cell antigen receptor signaling in p110delta PI 3-kinase mutant mice. Science 2002;297:1031-1034.
25. Dreyling M, Santoro A, Mollica L, et al. Phosphatidylinositol 3-kinase inhibition by Copanlisib in relapsed or refractory indolent lymphoma. J Clin Oncol 2017;35:3898-3905.
26. Ali K, Soond DR, Pin˜eiro R, Hagemann T, Pearce W, Lim EL, et al. Inactivation of PI(3)K p110d breaks regulatory T-cellmediated immune tolerance to cancer. Nature 2014;510:407e11. https://doi.org/10.1038/nature13444.
27. De Henau O, Rausch M, Winkler D, Campesato LF, Liu C, Cymerman DH, et al. Overcoming resistance to checkpoint blockade therapy by targeting PI3Kg in myeloid cells. Nature 2016;539:443e7. https://doi.org/10.1038/nature20554.
28. Tanaskovic O, Verga Falzacappa MV, Pelicci PG. Human cord blood (hCB)-CD34þ humanised mice fail to reject human acute myeloid leukemia cells. PLoS One 2019;14:e0217345. https://doi.org/10.1371/journal.pone.0217345.
29. Jassal B, Matthews L, Viteri G, Gong C, Lorente P, Fabregat A, et al. The reactome pathway knowledgebase. Nucleic Acids Res 2020. https://doi.org/10.1093/nar/gkz1031.
30. Nishimura D. BioCarta. Biotech Softw Internet Rep 2001. https://doi.org/10.1089/152791601750294344
31. Newman AM, Steen CB, Liu CL, Gentles AJ, Chaudhuri AA, Scherer F,

et al. Determining cell type abundance and expression from bulk tissues with digital cytometry. Nat Biotechnol 2019. https://doi.org/10.1038/s41587-019-0114-2

32. Aran D, Hu Z, Butte AJ. xCell: Digitally portraying the tissue cellular heterogeneity landscape. Genome Biol 2017;18:1 - 14. doi:10.1186/s13059-017-1349-1
33. Liu J, Lichtenberg T, Hoadley KA, et al. An Integrated TCGA Pan-Cancer Clinical Data Resource to Drive High-Quality Survival Outcome Analytics. Cell 2018;173:400-416.e11. doi:10.1016/j.cell.2018.02.052
34. Yong HJ, Choi Y, Joo HK, Chul WK, Jae MJ, Dong SL, et al. Immune response to firefly luciferase as a naked DNA. Cancer Biol Ther 2007. doi:10.4161/cbt.6.5.4005.
35. Becht E, Giraldo NA, Lacroix L, Buttard B, Elarouci N, Petitprez F, et al. Estimating the population abundance of tissue-infiltrating immune and stromal cell populations using gene expression. Genome Biol 2016. doi:10.1186/s13059-016-1070-5.
36. Bilanges B, Posor Y, Vanhaesebroeck B. PI3K isoforms in cell signalling and vesicle trafficking. Nat Rev Mol Cell Biol 2019. doi:10.1038/s41580-019-0129-z.
37. Motz GT, Santoro SP, Wang LP, Garrabrant T, Lastra RR, Hagemann IS, et al. Tumor endothelium FasL establishes a selective immune barrier promoting tolerance in tumors. Nat Med 2014;20:607 - 15. doi:10.1038/nm.3541.
38. Zhu J, Powis De Tenbossche CG, Cané S, Colau D, Van Baren N, Lurquin C, et al. Resistance to cancer immunotherapy mediated by apoptosis of tumor-infiltrating lymphocytes. Nat Commun 2017;8. doi:10.1038/s41467-017-00784-1.
39. Champiat S, Dercle L, Ammari S, Massard C, Hollebecque A, Postel-Vinay S, et al. Hyperprogressive disease is a new pattern of progression in cancer patients treated by anti-PD-1/PD-L1. Clin Cancer Res 2017;23:1920 - 8. doi:10.1158/1078-0432.CCR-16-1741.
40. Champiat S, Ferrara R, Massard C, Besse B, Marabelle A, Soria JC, et al. Hyperprogressive disease: recognizing a novel pattern to improve patient management. Nat Rev Clin Oncol 2018;15:748 - 62.

doi:10.1038/s41571-018-0111-2.
41. Kaneda MM, Messer KS, Ralainirina N, Li H, Leem CJ, Gorjestani S, et al. PI3Kγ is a molecular switch that controls immune suppression. Nature 2016;539:437 - 42. doi:10.1038/nature19834.
42. Kalbasi A, Ribas A. Tumour-intrinsic resistance to immune checkpoint blockade. Nat Rev Immunol 2019. doi:10.1038/s41577-019-0218-4.
43. Karam SD, Raben D. Radioimmunotherapy for the treatment of head and neck cancer. Lancet Oncol 2019;20:e404 - 16. doi:10.1016/s1470-2045(19)30306-7.
44. Lippitz BE, Harris RA. A translational concept of immuno-radiobiology. Radiother Oncol 2019;140:116 - 24. doi:10.1016/j.radonc.2019.06.001.
45. Demaria S, Coleman CN, Formenti SC. Radiotherapy: Changing the Game in Immunotherapy The promise of radiotherapy as a partner for immunotherapy 2017;2:286 - 94. doi:10.1016/j.trecan.2016.05.002.
46. Ngwa W, Irabor OC, Schoenfeld JD, Hesser J, Demaria S, Formenti SC. Using immunotherapy to boost the abscopal effect. Nat Rev Cancer 2018;18:313 - 22. doi:10.1038/nrc.2018.6.
47. Vanpouille-Box C, Alard A, Aryankalayil MJ, Sarfraz Y, Diamond JM, Schneider RJ, et al. DNA exonuclease Trex1 regulates radiotherapy-induced tumour immunogenicity. Nat Commun 2017;8:15618. doi:10.1038/ncomms15618.
48. Zhang X, Niedermann G. Abscopal Effects With Hypofractionated Schedules Extending Into the Effector Phase of the Tumor-Specific T-Cell Response. Int J Radiat Oncol Biol Phys 2018.;doi:10.1016/j.ijrobp.2018.01.094.
49. Dewan MZ, Galloway AE, Kawashima N, Dewyngaert JK, Babb JS, Formenti SC, et al. Fractionated but not single-dose radiotherapy induces an immune-mediated abscopal effect when combined with anti-CTLA-4 antibody. Clin Cancer Res 2009;15:5379 - 88. doi:10.1158/1078-0432.CCR-09-0265.
50. Barth RJ, Mule JJ, Spiess PJ, Rosenberg SA. Interferon γ and tumor necrosis factor have a role in tumor regressions mediated by murine CD8+ tumor-infiltrating lymphocytes. J Exp Med 1991;173:647 - 58. doi:10.1084/jem.173.3.647.

51. Seifert L, Werba G, Tiwari S, Giao Ly NN, Nguy S, Alothman S, et al. Radiation Therapy Induces Macrophages to Suppress T-Cell Responses Against Pancreatic Tumors in Mice. Gastroenterology 2016;150:1659-1672.e5. doi:10.1053/j.gastro.2016.02.070.
52. Thorpe LM, Yuzugullu H, Zhao JJ. PI3K in cancer: Divergent roles of isoforms, modes of activation and therapeutic targeting. Nat Rev Cancer 2015;15:7 - 24. doi:10.1038/nrc3860.
53. Aran D, Sirota M, Butte AJ. Systematic pan-cancer analysis of tumour purity. Nat Commun 2015;6:1 - 12. doi:10.1038/ncomms9971.
54. Ashley Hanlon and Danielle M. Brander, Managing toxicities of phosphatidylinositol-3-kinase (PI3K) inhibitors. Hematology 2020;1: 346 - 356.
55. David G. Winkler et al. PI3K-δ and PI3K-γ Inhibition by IPI-145 Abrogates Immune Responses and Suppresses Activity in Autoimmune and Inflammatory Disease Models. Chemistry & Biology 2013;20, 1364 - 1374
56. Zheng, Zhong et al. Efficacy and safety of duvelisib, a phosphoinositide 3 kinase (PI3K) [delta] and [gamma] inhibitor, in Chinese patients (pts) with relapsed/refractory follicular lymphoma (R/R FL): A single-arm, open-label, multicenter, phase II clinical trial. Journal of Clinical Oncology 2021;39(15_suppl):e19532
57. Dandan Meng, Wei He, Yan Zhang, Zhenguo Liang, Jinling Zheng, Xu Zhang, Xing Zheng, Peng Zhan, Hongfei Chen, Wenjun Li, Lintao Cai. Development of PI3K inhibitors: Advances in clinical trials and new strategies (Review). Pharmacological Research 2021;Volume 173:105900

국문초록

삼중음성유방암 모델에서 PI3Kγδ저해제와 방사선 병용치료를 통한 PD-1억제제의 항종양면역효과 극대화 전략

한민국

의과대학 협동과정 종양생물학

서울대학교 대학원

유방암은 면역원성이 부족하고, 면역억제성 종양미세환경을 가지고 있기 때문에 면역관문억제제에 대해 치료 저항성이 있다고 알려져 있다. 따라서 본 연구는 면역 억제를 방해하는 포스포이노시타이드 3-인산화효소 (phosphoinositide 3-kinase, PI3K) 저해제와 *in situ* 종양백신 효과를 유도하는 방사선치료 병용치료를 통한 PD-1억제제의 항종양면역효과를 극대화하고자 하였다.

면역세포를 온전히 가지고 있는 일반생쥐(BALB/c) 및 면역이 결핍된 생쥐(Nude)에서 유방암 세포주를 각각 성장시키고, 총 24 Gy 용량의 방사선을 3회로 나누어 성장된 종양에 조사하였다. 그리고 PD-1억제제와 PI3Kγδ저해제를 이틀에 한 번씩, 2주 동안 투여하였다. 종양 및 비장, 림프절을 추출하고 유세포분석 및 면역세포화학법을 이용하여 각 조직의

면역세포의 군집을 관찰하였다. 동일한 실험 일정으로 환자유래 인간화 마우스 (humanized patient-derived breast cancer xenograft, PDX) 모델에서 수행하였고, 실험 종료 후 종양조직에서 RNA를 추출하여 전사체분석을 통해 면역세포의 profile과 면역관련 pathways를 관찰하였다. 또한 Cancer Genome Atlas (TCGA) pan-cancer 코호트에서 전체사 및 임상적 자료를 수집하였고, deconvolution 알고리즘을 사용하여 면역세포의 repertoire를 확인하였다.

그 결과, PI3Kγδ저해제 및 방사선치료, PD-1억제제를 삼중병용치료한 군에서 종양의 성장이 유의미하게 지연되었다. 또한 방사선의 abscopal 효과가 증진되었고 생존률이 증가하였다. 단독 방사선치료는 $CD8^+$ T세포의 군집을 유의미하게 증가시켰지만, 동시에 조절T세포(regulatory T cells, Tregs)와 골수유래 면역억제세포(myeloid-derived suppressor cells, MDSCs) 및 M2 종양관련대식세포(tumor associated macrophages, TAMs)와 같은 면역억제성 세포의 군집 또한 함께 증가시켰다. PI3Kγδ저해제를 투여하였을 때에는 이러한 면역억제성 세포를 효과적으로 저해할 수 있었고 특히 삼중병용치료를 시행한 결과 종양, 비장 및 림프절에 존재하는 $CD8^+$ T세포 군집이 극적으로 증가하였다. 그리고 환자유래 인간화마우스 모델에서도 삼중병용치료가 종양성장의 지연시키고 면역억제성 pathways를 저해시킴을 확인하였다. 마지막으로 TCGA 코호트에서 Treg/$CD8^+$ T세포 및 M2/M1 TAM의 높은 분율과 환자의 낮은 생존률의 유의미한 연관성이 있음을 밝혔다.

이에 본 연구는 면역억제성 종양미세환경에서 PI3Kγδ저해제가 임상적으로 유의미한 타겟이라는 것과 방사선과 PD-1억제제의 병용은 면역억제성 종양 미세환경을 가진 유방암과 같은 면역적으로 “cold”한 종양의 치료 저항성을 극복할 수 있다는 가능성을 시사한다.

주요어 : 유방암, PI3K저해제, 방사선 치료, PD-1억제제, 면역항암제, Abscopal effect
학 번 : 2019-38319

감사의 글

하나님의 인도하심으로 박사 학위를 받게 되어 기쁘고 감사드립니다. 이 글을 읽는 모든 분에게 하나님의 사랑과 은혜가 가득하길 기도하고 저의 연구 결과가 이 글을 읽으시는 분들에게 조금이나마 보탬이 되기를 소망합니다.

연구를 통하여 암으로 힘들어하는 사람들에게 도움을 주고 사회에 공헌하겠다는 커다란 포부와 설렘으로 시작했던 박사학위과정이었는데, 고작 한 걸음 정도의 연구 결과와 조금의 아쉬움을 남기고 박사 학위의 끝을 맺게 되었습니다. 박사 학위 이후에도 비록 작은 한 걸음일지라도 꾸준히 멈추지 않고 연구자의 길을 걷겠습니다. 그리고 주변 사람들에게 좋은 영향력을 끼치는 과학자가 되고 싶습니다.

부족한 제가 박사 학위를 받을 수 있도록 도와주신 분들에게 이 자리를 통해 감사의 인사를 전해드립니다. 먼저 연구뿐만 아니라 크리스천으로서 본을 보여주시고, 박사 학위 기간 동안 아낌없는 지지와 지도를 해주신 김인아 교수님께 깊은 감사의 인사를 드립니다. 그리고 박사 논문 심사를 진행해주시고 연구의 방향을 올바르게 가도록 아낌없는 조언을 해주신 우홍균 교수님, 한원식 교수님, 박소연 교수님, 박경화 교수님께 감사를 전합니다. 앞으로 교수님들의 가르침에 따라 참된 연구자가 되도록 계속 노력하겠습니다.

연구실 동료들 덕분에 여기까지 올 수 있었습니다. 가장 가까운 곳에서 실험을 도와주신 강미현 선생님과 선배로서 도움을 주기는커녕 받기만 한 후배들 유민이와 성민이에게 고마움과 함께 좋은 추억들을 잘 간직하겠습니다. 그리고 함께 연구할 수 있어서 영광이었던 장원익 선생님, 장범섭 선생님, 위찬우 선생님께도 감사드립니다. 또한, 연구의 멘토이자 소중한 친구인 지운이와 종배, 미연이, 택진이, 지영이, 지수에게도 이 자리를 빌려 감사 인사를 전합니다. 이외에도 실험하며 도움을 주신 분들이 정말 많은데 모두 언급하지 못하여 죄송하고 정말 감사드립니다.

그리고 세상에서 제일 존경하고 과학자로서 또한 가장으로서 삶의 롤 모델이 되어 주시는 아버지와 나이가 많아졌어도 여전히 아이처럼 사랑만 주시는 어머니, 먼 나라 영국에서 꿈을 키우며 고생하는 잠룡이 내 동생 모두 사랑하고 감사합니다. 뿐만 아니라 박사과정 동안 새로운 가족이 된 믿음의 거장으로 롤모델이 되어 주신 장인어른, 항상 넘치는 사위 사랑 주시는 장모님, 멀리 뛰기 위해 도약을 준비하는 처남 모두 사랑하고 고맙습니다.

마지막으로 박사 학위의 시작과 끝을 함께해준, 그리고 앞으로의 생을 함께 걸어갈 아내 서경이에게 세상에서 제일 사랑한다는 진심이 담긴 말과 함께 이 논문을 바칩니다.